NASA Technical Memorandum 81841

A Preliminary Assessment of the Impact of 2-D Exhaust-Nozzle Geometry on the Cruise Range of a Hypersonic Aircraft With Top-Mounted Ramjet Propulsion

Walter A. Vahl and John P. Weidner

SEPTEMBER 1980

NASA

NASA Technical Memorandum 81841

A Preliminary Assessment of the Impact of 2-D Exhaust-Nozzle Geometry on the Cruise Range of a Hypersonic Aircraft With Top-Mounted Ramjet Propulsion

Walter A. Vahl and John P. Weidner
Langley Research Center
Hampton, Virginia

National Aeronautics
and Space Administration

**Scientific and Technical
Information Branch**

1980

SUMMARY

A theoretical study of full-length and shortened, two-dimensional, isentropic exhaust nozzles integrated with top-mounted ramjet-propulsion nacelles has been conducted. Both symmetric and asymmetric contoured nozzles with a range of angular orientations were considered. Performance comparisons to determine optimum installations for a representative hypersonic vehicle at Mach 5 cruise conditions are presented on the basis of cruise range, propulsive specific impulse, inlet area requirements, and overall lift-drag ratio. Aerodynamic trim was not considered. The effect of approximating the nozzle internal contours with planar surfaces and the determination of viscous- and frozen-flow effects are also presented.

INTRODUCTION

As aircraft cruising speeds increase toward hypersonic levels, the required propulsion system size increases relative to the aerodynamic lifting surfaces of the vehicle and assumes a more critical role in the configuration design process (ref. 1). Past studies of hypersonic configurations (refs. 1 to 4) have considered propulsion systems consisting of engine modules which are highly integrated with the vehicle undersurfaces. The module inlet is generally located to take advantage of the precompression afforded by the forward portion of the vehicle undersurface, thereby minimizing the inlet area, the mass, and the resultant drag penalties. The undersurface of the vehicle afterbody is also used for additional external exhaust-nozzle expansion and, hence, reduces the internal nozzle length and exit area of the module. Additionally, the high-pressure forces acting over the nacelle cowling and the gross-thrust vector each contribute significant force components to the aerodynamic lift.

Recently, the need to minimize the presence of the propulsion system relative to ground observation (ref. 5) has resulted in a new class of hypersonic vehicles being identified for application in the high-altitude low-hypersonic-speed regime. One of these vehicle concepts is characterized by ramjet-propulsion nacelles installed on an upper surface of the vehicle, possibly the wing, with inlets located in either free-stream or near free-stream flow. The arrangement of the nacelle on the wing upper surface appears to be quite similar to that of a nacelle mounted on the wing lower surface, but simply inverted. In this application, however, the nacelles become considerably larger, as a result of having inlets in free-stream flow without the benefit of precompression, and the exhaust nozzle is restricted to the nacelle itself. In addition, the inlet and nozzle surfaces may produce negative rather than positive lift components.

In order to assess the feasibility of using a nacelle mounted in an inverted position on top of a vehicle surface, a theoretical study was performed at the design cruise condition of a representative hypersonic aircraft to compare the effect on cruise-range performance of several nozzle installations

within the top-mounted nacelle arrangement. Each nacelle includes a free-stream inlet, a subsonic combustion chamber, and a two-dimensional (2-D) exhaust nozzle. Representative flight conditions of Mach 5 and a cruising altitude of 30.48 km have been selected. Since the inlet is considered to be located in the free-stream flow (which will be the main factor affecting its size), major emphasis will be placed on the problem of integrating a two-dimensional exhaust nozzle into a complete propulsion package so as to obtain an optimized top-mounted nacelle. Representative values will be assumed for the inlet pressure recovery and the ramjet combustor efficiency in order to determine the exhaust-nozzle throat conditions. The effect on aircraft cruise-range performance of such propulsion system design variables as length, orientation, and geometry of the exhaust nozzle will be examined for a representative set of hypersonic vehicle aerodynamics.

SYMBOLS AND ABBREVIATIONS

A	area, m^2
AI	asymmetric, inverted
AU	asymmetric, upright
C_D	drag coefficient, D/qS_w
C_L	lift coefficient, L/qS_w
C_T	thrust coefficient, F_v/qS_w
D	drag, N
F	force, N
g	acceleration due to gravity, 9.807 m/s^2
h	height, m
I_{sp}	specific impulse, F_v/mg, s
ℓ	length, m
L	lift, N
L/D	lift-drag ratio
$\dot{m}$	fuel mass flow per unit time, kg/s
p	pressure, Pa
q	dynamic pressure, Pa
R	cruise range, km

S	reference area, m^2
SY	symmetric
T	temperature, K
V	velocity, m/s
W	vehicle mass, kg
X,Y	reference coordinates, m
α	angle of attack, deg
γ	ratio of specific heats
ν	nozzle internal-flow turning angle, deg
ρ	density, kg/m^3

Subscripts:

1	beginning of cruise
2	end of cruise
c	cowl
g	gross
i	inlet
L	lift direction
lim	limit
n	nozzle
r	ram
ref	reference
s	surface
t	throat
v	free-stream velocity direction
w	wing

x,y	reference coordinates
∞	free-stream conditions

PROPULSION SYSTEM DESIGN FACTORS

Arriving at an efficient ramjet-propulsion-system design that permits a vehicle to achieve its cruise mission requirements involves a compromise between many conflicting variables. The cruise altitude, the flight speed, and the location of the inlet in the flow field, along with the compression-process efficiency and the degree of variable geometry, will all influence the inlet size, mass, and drag. In addition, the ramjet burner must be able to accommodate the required airflow over the speed range. The exhaust nozzle can also have a large effect on the final performance, drag, and mass of the overall propulsion system. The exhaust-nozzle design and the method of its integration into the nacelle will influence not only propulsive performance but will also affect the outer nacelle shape and the direction of the thrust vector. Factors such as contouring of the internal nozzle surface, viscous flow effects, and the state of the expanding exhaust gases (whether it approaches equilibrium or frozen) will influence the overall nozzle-design process and the resulting propulsive performance.

The purpose of this paper is to examine the influence on the vehicle cruise performance of the geometry of a two-dimensional nozzle integrated into a top-mounted nacelle (fig. 1). In this regard, three nozzle-integration geometries were considered and are illustrated in figure 2. These geometries include an inverted asymmetric (AI) nozzle, an upright asymmetric (AU) nozzle, and a symmetric (SY) nozzle. In previous studies of hypersonic propulsion integration, an upright asymmetric nozzle was typically combined with a bottom-mounted nacelle to produce both thrust and lift. Simply inverting the nacelle and its nozzle implies a negative component of lift, which would reduce a vehicle's lift-to-drag ratio and cruise performance. However, the inverted nozzle does appear to be the most volume-efficient concept for applications which may require including a turbojet engine below the ramjet for low speed thrust, as shown in reference 6.

In addition to comparing performance of the three nozzle concepts illustrated in figure 2, other factors were assessed, such as nozzle length, gross-thrust vector orientation, nozzle internal-surface contouring, viscous-flow effects, and the assumed state of the exhaust gases. The resulting propulsive performance data were combined with the aerodynamic performance calculations for a hypersonic aircraft configuration to assess the impact of nozzle changes on cruise range.

STUDY GUIDELINES

Approach

In order to make comparisons of the performance of a large number of potential nozzle/nacelle installations, some logical procedure must be adopted for

constraining some of the many variables present. The general approach of this study was to assume fixed values (given in appropriate subsections) for some of the gross, basic, aerodynamic and propulsion-system parameters considered representative of this class of hypersonic vehicle. Use of these assumed constant values allowed detailed parametric consideration to be given to the exhaust-nozzle integration. Trade-offs could then be made to determine optimum nacelle/nozzle installations. Additionally, since the intent of the study is a preliminary assessment of nacelle/nozzle combinations installed on vehicle upper surfaces, the positioning of the nacelles relative to a particular aerodynamic configuration is not defined, and hence, pitching moments and trim considerations were not addressed. The nacelle/nozzle could conceivably be mounted on such upper surfaces of a vehicle as the fuselage or wing, with or without supporting pylons. If it can be shown in a preliminary study that top-mounted nacelles with two-dimensional exhaust nozzles present a viable propulsion-system concept, then the next step in the design process would be integration of the nacelle with a vehicle having a specific mission requirement. At this point in the design process, the pitching moment and trim considerations for the particular configuration would be addressed.

Propulsion Nacelle Description

To integrate the exhaust nozzles under consideration with a nacelle, the following ground rules were established. Cruising conditions were assumed to be Mach 5 at an altitude of 30.48 km. The nacelle was considered to be installed on the upper surface of a wing, with the wing having a flat undersurface which is typical of this class of hypersonic vehicles. As shown in the schematic of the nacelle (fig. 3), the nacelle lower surface was assumed to be fixed at a constant angle of 6° relative to the free-stream flow direction. The inlet was considered to be operating in free-stream flow at full capture and to be aligned with the free-stream direction. The length of the wing chord at the nacelle location was equal to nine inlet heights.

The nacelle was held at a constant angle of 6° to permit the nozzle throat conditions and the lower nacelle geometry to be held constant throughout the study. The calculation of balanced forces at cruise flight conditions required that the vehicle angle of attack deviate a small amount, causing a discontinuity between the wing and the bottom of the nacelle. However, it was felt that the effect would be small and could be discounted within the scope of the present study. The final orientation of the nacelle relative to the vehicle surfaces would, in itself, be another iteration in the design process.

The axial position of the upper corner of the exhaust-nozzle throat was located at the station of the wing trailing edge. The throat height was equal to 0.1658 of the inlet height (fig. 3). In addition, the end point of the bottom surface of the nozzle, as installed in the nacelle, was located on a plane which was aligned with the free-stream flow and passed through the trailing edge of the wing. This imposed limit prevented any of the nozzle lower surface from

projecting below the wing into the free-stream flow. In order to determine the optimum thrust vector angle, each nozzle considered was installed in the nacelle with several angular orientations. The angular orientation, length, and internal surface contour of the nozzle determined the vertical location of the nozzle throat.

The nacelle cowling began at the inlet-cowl lip, as shown in figure 3, and consisted of four planar panels. The first three panels had lengths of 0.6, 0.9, and 0.7 of the inlet height, respectively, with the last panel extending to the end point of the top surface of the nozzle. In addition, a minimum cowl-wall thickness of 0.04 of the inlet height was specified at the nozzle throat station. For some of the angular nozzle orientations where the cowl exit would tend to fall below the last panel, an additional section was added to extend from the nozzle throat station to the end of the nozzle cowl. In figure 2, the upper nacelle illustrates a nozzle installation where five cowl panels were required. The middle and lower installations represent nozzle orientations where only the four cowl panels were required. The three initial cowl-panel surfaces were specified at angles relative to the free-stream flow direction of 9.5°, 2.5°, and -3°, respectively.

Exhaust-Nozzle Throat Conditions

Since the major emphasis in this study is centered on the performance of the exhaust nozzle and its integration with the ramjet nacelle, representative exhaust-nozzle throat conditions were required as a beginning point for subsequent calculations of nozzle performance. A one-dimensional cycle program (ref. 7) was utilized to perform equilibrium, real-gas, ramjet internal-flow calculations. The inlet was assumed to be operating at full mass-flow capture with a kinetic efficiency of 0.925 in free-stream Mach 5 flow at an altitude of 30.48 km. The ramjet burner calculations were based on the following combustor conditions: an entering velocity of Mach 0.2, a hydrogen-air mixture having a fuel equivalence ratio of 0.6, and an overall combustion efficiency of 0.95. The selected value of fuel equivalence ratio was considered a typical, throttled ramjet condition which would allow a sufficient thrust margin at cruise for maneuvering and for altitude excursions. After combustion, the flow entered the exhaust nozzle through a sonic throat. The cycle calculations gave values of throat pressure ($p/p_{\infty} = 105.4$), temperature ($T/T_{\infty} = 9.4$), and cross-sectional area ($A/A_i = 0.1658$) which were held constant for all subsequent two-dimensional exhaust-nozzle calculations. The ramjet cycle program utilized an isentropic, equilibrium, real-gas expansion process so that the value of the ratio of specific heats for the exhaust gases varied throughout the nozzle length. However, the computer program used for the subsequent two-dimensional exhaust-nozzle calculations (refs. 8 and 9) required a constant value of the ratio of specific heats. To permit approximation of the equilibrium flow in the two-dimensional nozzle calculations, a value of the specific heat ratio ($\gamma = 1.30$) was determined which matched the exit area and pressure of the fully expanded nozzle in the ramjet cycle analysis.

Description of Exhaust Nozzles

Two basic types of two-dimensional (2-D) exhaust nozzles were considered for integration with the nacelle. A sketch representing each type of nozzle is shown in figure 4.

The SY nozzle has equal amounts of internal flow turning on both the upper and lower surfaces, with the length of the nozzle defined by the intersection of the last expansion wave with the opposing surface. The internal surface of the nozzle had reflexed contours to cancel all reflections of the expansion Mach waves as they intersected the opposing surfaces so that the resulting exit flow was uniform and parallel.

The AI nozzle is essentially one-half of the SY nozzle with all dimensions doubled and the SY nozzle centerline replaced with a cowl internal surface having an angle of 0°. Because of the unsymmetrical nature of this nozzle, a normal force is produced for nozzles having less than full expansion which, when combined with the axial force, yields a gross thrust greater than that of the symmetric nozzle. The length of the cowl is defined by the last expansion wave of the initial lower-surface expansion fan. The initial expansion-fan waves reflect from the upper cowl surface and are cancelled when they reach the reflexed lower surface of the nozzle yielding uniform, parallel exit flow across the nozzle exit plane. The nozzle length is defined by the point where the last Mach wave reflected from the cowl intersects the nozzle lower surface.

A basic parameter governing the performance of supersonic exhaust nozzles is the total amount of internal flow turning (that is, the cumulative degrees of supersonic flow turning experienced by a flow streamline as it passes from the nozzle throat to the nozzle exit plane). A series of computer calculations were performed for a range of nozzle-design parameters in order to gain insight into the relationship of exhaust-nozzle gross-thrust performance to total internal flow turning, length, and surface area of a nozzle and the relationship between fully expanded nozzles with uniform flow and shortened nozzles with exit-flow divergence. The results of this investigation are presented in the appendix. Under the conditions assumed, nozzles fully expanded to free-stream ambient pressure would require total internal flow turning of 74.8°. However, based on the gross-thrust performance trends shown in the appendix, there is only a slight gain in performance to be realized over the final half of the fully expanded nozzle length. Accordingly, two representative nozzles having total internal-flow turning of 64° and 72° were selected for each of the SY, AI, and AU nozzle types for further study of their applicability for integration with the ramjet nacelle. These nozzles correspond to initial throat-turning angles of 32° and 36°, respectively. The Method of Characteristics (refs. 10 and 11) was used, with a constant ratio of specific heats of 1.30, to define internal contours of the nozzle. For nozzles with 64° and 72° of internal-flow turning, the full-length nozzle with uniform, parallel exit flow and shortened versions with reduced total internal turning and exit-flow divergence were integrated with the nacelle.

PERFORMANCE CALCULATION METHODS

Nacelle Force-Accounting Procedures

In order to determine the overall forces acting on the nacelle for the various exhaust-nozzle installations resulting from the variety of nozzle shapes, lengths, and orientation angles, the forces acting on the individual nacelle components were integrated for each specific nozzle considered and their contribution in the vehicle lift and drag directions were determined. A sketch of the nacelle showing the forces present and the equations used to calculate them is shown in figure 5.

Since the inlet is operating in free-stream flow at full capture, the force acting at the inlet-plane airstream is simply the ram drag or the momentum of the entering flow. The forces acting over the external surface of the nacelle cowl were calculated by integration of the local surface pressures resulting from either the two-dimensional shock waves or the Prandtl-Meyer expansion flow over each individual cowl panel. Viscous effects were not determined. In addition, the minimum static pressure due to the expanding flow over the rearmost surface panels was limited to 0.3 of the free-stream static pressure, since it was felt that pressures below this value, while theoretically possible for 2-D flow, would not be attained in actual installations because of viscous effects limiting the amount of expansion that can take place.

The inviscid pressure forces acting over the upper and lower inner surfaces of the exhaust nozzles were integrated using the nozzle computer program described in the appendix, and the resulting force components in the axial and normal direction were determined.

To complete the nacelle force accounting, the thrust force acting at the nozzle-throat entrance was calculated as the momentum of the combustion streamtube plus the force due to the pressure acting over this streamtube area. All pressure forces used in the force-accounting procedure were referenced to free-stream static pressure.

Range Calculations

In order to assess range performance, a typical hypersonic-cruise mission was postulated for a turboramjet-powered vehicle. The aerodynamic data for the vehicle at Mach 5 are shown in figure 6 and are considered representative of a hypersonic-cruise vehicle based on in-house analytical studies.

To determine the effect on the cruise range of cumulative mass changes resulting from the large variation of nozzle installations, the baseline values shown in table I were assumed. The nacelle propulsion forces were integrated with the aerodynamic forces, and through an iterative procedure, the required inlet area and vehicle aerodynamic angle of attack, with all forces balanced at cruise, were determined. Once the proper values were established, the cruise range was calculated using the standard Breguet range equation $\left[R = (VI_{sp}L/D) \ln (W_1/W_2)\right]$ and available cruise fuel.

A typical range calculation proceeded as follows. The specific nozzle being considered was oriented in the propulsion nacelle at a specified angle with respect to the nacelle reference line. An initial inlet capture area and vehicle angle of attack were assumed, and the total nacelle forces in both the vehicle lift and drag directions were determined. The change in nozzle surface area from that of the nominal nozzle permitted an increment in nozzle mass to be determined, while the total ramjet mass was adjusted for the resizing required for thrust to equal drag. Thus, a new takeoff gross mass and turbojet-system mass were determined. This new takeoff gross mass and the prescribed acceleration-fuel requirement resulted in a new value for the beginning-of-cruise mass. For this new mass, the required aerodynamic C_L and inlet area could be determined and compared to the previous values. The inlet area was iterated until the proper value was found which resulted in all forces being balanced at the cruise condition. The Breguet cruise range was then calculated using the overall effective L/D, the propulsive I_{sp}, and the fuel remaining after the required acceleration fuel was subtracted from the fixed total fuel available.

RESULTS AND DISCUSSION

Cruise-Range Performance

Orientation of nozzles.- In order to find an optimum cruise performance, each of the nozzles considered was rotated through a range of angles relative to the inlet, from 0° to 20° with respect to the flight direction, to change the direction of the thrust vector. A typical shortened version of the 64° total turning AI nozzle, which has 54° of indicated flow turning, is shown in figure 7 at three different orientation angles. The lift and thrust forces produced by the nacelle and nozzle are given in figure 8 and are representative of all of the nozzles considered. The gross thrust is the dominant force, while the nacelle outer drag represents only a small fraction of the net thrust. By rotating the nozzle orientation angle, the component of gross thrust in the flight direction is reduced (resulting in a lower propulsive I_{sp}), and a component of lift is derived. These forces are combined with the basic aerodynamic forces of the vehicle in order to determine cruise-range performance using the method described in the previous section.

Effect of shortening nozzles.- The cruise-range performance for the full-length and shortened versions of the 64° total internal-turning nozzles is shown in figure 9 for all three nozzle types, while the performance for the full-length and shortened versions of the 72° total internal-turning nozzles is shown in figure 10. Performance is plotted against gross-thrust vector angle and is given in terms of propulsive I_{sp} in the flight direction, overall integrated L/D (including thrust-vectoring effects), inlet-cowl area required for a 60-percent power setting at cruise, and the resulting cruise range. Additionally, the angular differences between the gross-thrust vector and the nozzle orientation angle, as well as the internal surface area, are presented in tabular form for each nozzle. The various nozzles are defined in terms of the total internal-flow turning present in the nozzle, excluding any flow-divergence effects. These data include the effects of changing nozzle surface on the overall vehicle mass.

It is readily apparent from figures 9 and 10 that vectoring the gross thrust has a considerable beneficial influence on both the maximum cruise range and the minimum inlet area achieved, with the optimum-thrust vector generally being approximately 10°. The long versions of the AI nozzles (figs. 9(a) and (b) and 10(a), (b), (c), and (d)) have reduced range performance because of the imposed ground-rule restriction that the end point of the nozzle bottom surface be located on a plane aligned with the free-stream and passing through the trailing edge of the wing. This restriction forced the nozzle-throat location, fixed horizontally at the wing trailing edge, upwards. This resulted in a nacelle cowling with considerable compression surface area exposed to the free-stream and thereby caused excessive nacelle-cowling pressure-drag forces. For these nozzles, the cowl forces dominate performance and are in contrast to the small nacelle-cowl forces illustrated in figure 8, which represent a much smaller nozzle size. As the nozzles were shortened, the AI-nozzle performance generally attained the level of the AU and SY nozzles. The longest versions of the AU nozzles (figs. 9(a), (b), and (c) and 10(a) and (b)), on the other hand, showed an advantage over the SY and AI nozzles. This resulted from the additional lift component derived from the long AU-nozzle surface area permitting the vehicle to have a lower aerodynamic-lift requirement with a lower angle of attack and, hence, less drag. The gain in lift with these nozzles, for the assumed nozzle mass per unit surface area, was more beneficial than the decrement in vehicle mass and acceleration-fuel requirements resulting from the increased nozzle surface area. These trends for the long versions of the AU and AI nozzles emphasize the fact that the results of any propulsion-nacelle integration study can be very sensitive to the method of installation chosen and to the ground rules assumed. Care must be exercised in the interpretation of the overall study results.

Optimum performance based on nozzle surface area.- The optimum range performance for each nozzle of figures 9 and 10 has been plotted in figure 11 as a function of the nozzle internal surface area in order to compare the range performance of the various lengths and types of nozzles. The nozzle mass increments and the cooling requirements attendant to varying the nozzle length make the internal surface area a critical parameter in evaluating overall range performance. The values for the nozzle surface area have been nondimensionalized by the inlet-cowl area. Sketches of the three optimum-performance nozzles are also shown (fig. 12).

Comparison of the optimum range performance for installations of the 64° and 72° turning full-length and shortened nozzles shows that the 72° turning SY nozzle, shortened to approximately 65° of internal turning, results in the maximum range for the least nozzle internal-surface area. This range is 19 percent greater than the range achieved with the typical moderate sized AI nozzle (given in figs. 7 and 8) having a zero thrust-vector angle. The wide range in performance achieved shows the importance and sensitivity of the nozzle integration procedure on the overall mission performance. The 72° turning AU nozzle achieves a cruise-range performance similar to the 72° turning SY nozzle but has a one-third increase in internal surface area, which may impose a performance penalty when considering nozzle cooling requirements. The 64° and 72° turning AI nozzles attain a cruise range that is 4 percent less than the SY and AU nozzles but have a somewhat lower nozzle surface area at optimum performance.

Based on the cruise-range levels achieved for the various nozzle/nacelle arrangements, it appears feasible, within the study ground rules, to integrate a free-stream inlet and a two-dimensional exhaust nozzle into an upper-surface-mounted ramjet nacelle.

Effect of nozzle weight on performance.- The shapes of the performance curves given in figure 11 are strong functions of the mass penalties associated with changing the nozzle size and geometry. To gain an appreciation of the effect of the nozzle mass on performance, calculations were made for the full-length and shortened 72° turning nozzles using nozzle masses per unit internal surface area of 97.65 and 146.47 kg/m^2 in addition to the nominal value of 48.82 kg/m^2 used in the study. The effect on the optimum range performance is shown in figure 13, and as expected, the cruise ranges decrease with increasing nozzle mass. The maximum cruise range is achieved using the SY nozzle for each of the masses considered, while the AI nozzle exhibits the smallest range decrements. For nozzles weighing three times more than those used in the study (146.47 vs 48.82 kg/m^2), the AI nozzle has a decrement in optimum range of only 1.7 percent, while the AU and SY nozzles have range decrements of 5.0 percent and 3.0 percent, respectively. It is noteworthy that, as the nozzle mass increases, the optimum cruise-range performance of the AI and AU nozzles approach each other. The nominal mass penalty used for nozzles in this study is 48.82 kg/m^2 of nozzle internal-surface area and is amplified to 67.40 kg/m^2 when the impact of mass increases on the turbojet and ramjet engines are considered. Additional mass penalties brought about by variable-geometry and cooling considerations, along with other factors that might not have been considered in this study, would tend to negate the performance advantage of the long AU nozzles. For nacelle installations in which a short nozzle must be installed because of configuration restrictions, the shortened SY nozzle appears as the preferred candidate for achieving maximum performance with a minimum of nozzle length and internal-surface area.

Range performance is reduced by fully expanding the exhaust-nozzle flow to free-stream ambient pressure, as can be seen by examining the trend of the ranges achieved in figures 11 and 13 at the higher values of S_n/A_i. Increasing values of S_n/A_i correspond to longer nozzles having greater amounts of internal flow turning with the flow expanded more nearly to the free-stream ambient pressure. Additional calculations were made to determine the impact of simplified nozzle geometry and real-gas flow on performance.

Planar-Surface Nozzle Approximations

By using the nacelle with a 64° AI nozzle shortened to 54° of indicated flow turning as a reference, several, simple planar-surface approximations to the contoured internal nozzle surface were made to evaluate the effect on cruise-range performance. Use of planar internal nozzle surfaces would result in considerable reduction of fabrication cost and complexity of the nozzle installation and, in addition, would facilitate the incorporation of variable nozzle geometry for thrust vectoring over the vehicles operating envelope. Sketches of the nozzle-surface approximations which were considered are shown in figure 14.

The simplest approximation of the nozzle internal surface is to use one planar surface extending from the nozzle throat to the nozzle end point, which results in an angle of 20.3° as shown in the upper sketch. A closer approximation to the contoured nozzle wall is obtained by using two planar surfaces as shown in the two middle sketches. The surface referred to as the midpoint surface starts at the nozzle throat at an angle of 26° and intersects the contoured wall at approximately the nozzle-length midpoint. A 13.7° planar surface then extends to the endpoint of the nozzle. The surface referred to as the slope-intercept surface extends two planes, each tangent to the contoured nozzle surface at the throat and nozzle endpoints and forming angles of 32° and 12°, respectively, which intersect each other below the contoured nozzle surface. The lower sketch is a one-planar-surface approximation to the contoured nozzle which is at an angle of 28° and results in a nozzle having a considerably larger exit area than the contoured nozzle.

The cruise performance using the nacelles containing the planar-surface nozzle approximations is shown in figure 15. The best approximation, of those considered, is the midpoint nozzle using two planar surfaces, which attains a maximum range performance reduced approximately 1.5 percent from that obtained with the contoured nozzle. The simplest approximation, one planar surface, results in a value for the maximum range-performance parameter approximately 5 percent below that obtained with the contoured nozzle. The nozzle approximations using the slope intercept and increased exit-area surfaces attain range-performance values approximately midway between the nozzles using the midpoint and one-planar surfaces. For some applications, the simplification and additional nozzle versatility resulting from the use of planar-surface exhaust nozzles may offset the relatively small losses in range performance. Detailed trade-off studies would have to be conducted to evaluate each particular installation.

Viscous- and Frozen-Flow Effects

Since all of the previous nozzle/nacelle analyses considered inviscid, isentropic flow (γ = constant = 1.30), the 64° AI nozzle shortened to 54° of indicated flow turning was selected to assess the effects on cruise performance of nozzle operation with representative viscous and frozen flow. The viscous forces were evaluated from the shear forces obtained by using a Spalding-Chi calculation and by assuming the following nozzle parameters derived from in-house exhaust-nozzle analyses: a Reynolds number per meter of 9.84×10^5, a nozzle wall temperature of 333 K, a Prandtl number of 0.7, and a virtual origin 1.524 m ahead of the nozzle throat. As an approximation of frozen-flow conditions, the exhaust gases were considered frozen at the nozzle throat and a value of the ratio of specific heats of 1.24 was assumed constant throughout the nozzle. Based on tabulations in reference 8, this value (γ = 1.24) was chosen as representative of a lower bound on the specific heat ratios for frozen flow at the assumed throat conditions over a range of fuel equivalence ratios.

The cruise-range performance data for the nozzle with viscous and frozen exhaust flow is presented in figure 16. The viscous effects on the optimum range performance results in a 2.7 percent reduction from the reference

isentropic-flow condition. Addition of frozen-flow effects introduces an additional loss in range of 2.3 percent for a total range reduction of 5.0 percent. For comparative purposes, the performance of the simplest planar-surface approximation to the contoured nozzle, consisting of one planar surface from the nozzle throat to the nozzle-surface endpoint, is shown assuming both viscous and frozen flow. This nozzle-range performance is approximately 10.5 percent below that of the contoured isentropic-flow nozzle and gives an indication of the magnitude of the cruise-range performance loss incurred due to both simplification of the nozzle surface contours and consideration of "real-gas" effects.

CONCLUSIONS

A study has been conducted to determine the relative merits of integrating various two-dimensional exhaust nozzles with a ramjet nacelle mounted on the upper surface of a vehicle cruising at Mach 5 with a free-stream inlet. A force-accounting procedure was used to sum the inlet ram-drag effects, the external pressure forces over the nacelle surfaces, and the exhaust-nozzle gross-thrust vectoring to determine the optimum orientation of the nozzle installation for maximum cruise-range performance. Force moments and any required trim effects were not addressed because the present study was considered preliminary. Trim consideration would require a specific aerodynamic configuration and propulsion system installation and represents a further iteration in the overall design procedure. Careful consideration must be given to the effects on final cruise-range performance of the assumed study ground rules and any imposed vehicle installation restrictions when evaluating the relative performance of the various nozzle shapes and lengths. From the results of the analysis, the following points are considered significant:

1. Based on the cruise-range levels achieved, it appears feasible, at cruise conditions of Mach 5 and 30.48 km altitude, to integrate a free-stream inlet and a two-dimensional exhaust nozzle into an upper-surface-mounted ramjet nacelle.

2. On the basis of minimum internal-surface area, the two-dimensional exhaust nozzle achieving the maximum cruise-range performance, within the assumed study guidelines, was a symmetric nozzle designed for 72° of total internal turning which was shortened by eliminating a number of the final expansion waves to give approximately 64° to 66° of internal turning. The same cruise-range performance was achieved with a 72° total turning upright asymmetric nozzle shortened to 66° of turning, but the wetted internal-surface area of the nozzle increased by 33 percent.

3. The optimized maximum range of the three types of nozzle/nacelle installations considered was within approximately 4 percent of each other.

4. Range performance is reduced by fully expanding the exhaust-nozzle flow to free-stream ambient pressure; the slight gain in gross-thrust performance being more than offset by the large increase in wetted internal-surface area of the nozzle and the attendant mass penalties.

5. Simplification of the nozzle internal contour by using an approximation consisting of two planar panels resulted in an approximately 1.5 percent reduction in the maximum cruise range for the 64° asymmetric inverted nozzle shortened to 54° of indicated flow turning. Further simplification, by using only one planar panel, resulted in approximately a 5 percent loss in the maximum cruise range.

6. An evaluation to determine viscous and frozen chemistry effects resulted in a 2.7 percent decrease in the maximum range when considering the flow to be viscous and a 5.0 percent reduction when considering the flow to be both viscous and frozen at the nozzle throat for a 64° inverted asymmetric nozzle shortened to 54° of indicated flow turning.

National Aeronautics and Space Administration
Langley Research Center
Hampton, VA 23665
July 31, 1980

APPENDIX

EFFECTS OF INTERNAL FLOW TURNING ON PERFORMANCE OF NOZZLES WITH UNIFORM FLOW AND WITH FLOW DIVERGENCE

Exhaust-Nozzle Performance Calculations

Calculation procedures.- In determining the forces acting on the internal surfaces of the nozzles under consideration, use was made of a computer program designed to calculate two-dimensional supersonic flows (γ = constant) including the formation of shock waves and the external plume resulting from the interaction of the nozzle flow with the external flow field. The computing procedure involves both finite-difference downstream "marching" and floating shock-fitting techniques. A description of the methods used in the computer program can be found in references 9 and 12.

The nozzle internal forces were determined by integrating the pressure forces acting over the internal surfaces of the nozzle. The nozzle internal-surface contours were supplied as input for each of the nozzles considered. In order to determine a suitable grid spacing to be used in the computer-program numerical analysis, several computer calculations were made for a nozzle with isentropic, uniform, parallel exit flow over a range of grid spacings. The resulting internal nozzle forces were then compared to the ideal-nozzle thrust forces calculated using the flow tables of reference 13 for the same throat conditions and amount of total, internal flow turning. Shown in figure 17 are the results of the various grid spacings on the nozzle gross thrust as calculated with the computer program. The results are shown as the deviation of the nozzle computer-program force values from those computed using the tabulated ideal flow values. As the input grid spacing decreases, the computer-program force values asymptotically approach within approximately 0.6 percent of the ideal value calculated using the flow tables. Agreement of approximately 0.6 percent of gross thrust results in about a 2 percent agreement in net thrust, which was considered acceptable for numerical analyses of this nature. From computing-time and expense considerations, a grid spacing of 75 points at the nozzle throat was used for all subsequent nozzle calculations.

Nozzle lengths and internal surfaces.- In order to determine the exhaust-nozzle lengths and to define the internal-surface contours of the nozzles selected to investigate effects of nozzle length reduction, detailed layouts of isentropic nozzles having uniform, parallel exit flows were made using the Method of Characteristics. Only AI and AU nozzles were defined since the SY nozzles would be mirror images of the AI and AU nozzles with all dimensions halved as shown in figure 4. A discussion of the procedures involved in utilizing the Method of Characteristics can be found in references 10 and 11. The nozzle flows were defined using 4° wave-spacing increments. Accuracy of the nozzle layouts were verified by comparing the exit areas of the fully expanded nozzle determined in the layouts with those determined by theoretical calculations using flow tables (ref. 13). A representative layout and internal-surface contour for a 64° turning AI nozzle is shown in figure 18. Total internal turning of 74.8° (γ = 1.30) is required for a full-expansion nozzle

at the cruise conditions chosen for this study. Shown in figure 19 are the lengths and internal-flow wetted surface areas of the nozzles over the range of total internal-flow turning considered. The values have been nondimensionalized by the appropriate values of a reference, 64° total turning, AI nozzle. For the same throat height and total internal-flow turning, the SY nozzle is only one-half as long as the AI and AU nozzles and has less internal surface area.

Uniform-Flow Nozzle Performance

In order to gain preliminary insight as to the variation of exhaust-nozzle gross thrust with the basic design variables of nozzle length and internal-flow wetted surface area, calculations were performed for the SY, AI, and AU nozzles of figure 19 having amounts of total internal-flow turning which ranged from an underexpanded value of 20° to a value of 74.8°, which corresponded to a full expansion to free-stream ambient pressure. Each nozzle had isentropic, uniform, parallel exit flow.

The gross-thrust performance of the isentropic nozzles is shown in figure 20. All values have been nondimensionalized by the appropriate values corresponding to the reference AI nozzle having 64° of total internal-flow turning. The upper figure shows the gross-thrust performance as a function of the total nozzle length and clearly distinguishes the SY nozzle as superior from this standpoint. However, based on internal surface area, which is indicative of mass and cooling requirements, the lower figure shows the longer AI and AU nozzles to have an advantage over the SY nozzle in most instances. This is a result of eliminating the lift vector for the SY nozzle, as was discussed in reference to figure 4. Another factor of interest, which is readily observable in figure 20, is that there is little benefit to be derived in attempting to fully expand the nozzle flow to the free-stream ambient pressure. Expanding the flow from 64° of internal turning to the fully expanded turning value of 74.8° results in a gross thrust increase of approximately 0.5 percent over that of the reference AI nozzle, while more than doubling the nozzle length and surface area. Based on the gross-thrust performance trends, the 64° and 72° total internal turning nozzles for the AI, AU, and SY nozzles were selected for investigating the effect on performance of shortening the nozzle length with resultant exit-flow divergence.

Performance of Shortened Nozzles With Flow Divergence

Procedure for shortening nozzles.- The procedure used in defining reduced-length versions of the 64° and 72° internal turning nozzles was to delete a number of the final-expansion Mach waves at the exits of the two types of nozzles by cutting the nozzle off along a selected expansion wave, thereby decreasing the total amount of internal flow turning and reducing the nozzle upper- and lower-surface lengths. For the SY nozzle, the upper and lower lengths were reduced an equal amount. For each of the shortened nozzles, the exit flow was no longer parallel and uniform over the entire nozzle exit plane but incurred greater flow divergence for a shorter nozzle. Shown in figure 21 are the relative amounts of the nozzle-exit-plane area affected by the diverging flow for

the shortened versions of the 64° total turning, uniform, parallel exit flow, AI nozzle. As the nozzle is shortened by eliminating a number of the final-expansion Mach waves, the total internal-flow turning indicated is achieved along the last expansion wave that lies below the expansion fan that originates from the nozzle throat. In the upper region of the nozzle, approaching the cowl surface, the expansion turning angle is reduced and the direction of the flow becomes aligned with the cowl surface. For an indicated expansion angle of 42°, the flow direction in the bottom portion of the nozzle is downward, at an angle of 22° from the axial direction, and the region of flow divergence is 28 percent of the projected exit area. Several shortened versions of both the 64° and 72° turning full-length nozzles were considered for the AI, AU, and SY nozzles. Sketches of the wall contours of shortened versions of the 64° turning full-length AI nozzle are shown in figure 22.

The wetted internal areas of both the full-length and shortened versions of the AI, AU, and SY nozzles are shown in figure 23. The values of wetted area have been nondimensionalized by the wetted area of the reference, full-length 64° turning AI nozzle.

Performance comparison.- The gross-thrust performance of the shortened versions of the 64° and 72° turning nozzles is compared in figure 24 to the performance of a series of full-length, uniform, parallel-exit-flow nozzles for the AI, AU, and SY nozzles. The comparison is based on the amount of nozzle surface area exposed to the internal flow and covers a range of internal flow turning from approximately 42° to 72°. The values have been nondimensionalized by the appropriate values for the reference, uniform, parallel-exit-flow AI nozzle having 64° of total internal-flow turning.

For the AI, AU, and SY nozzles, it is seen that, for a given gross-thrust requirement, there is a significant reduction in the internal-flow wetted area when utilizing a shortened nozzle. The shortened nozzle has a higher initial throat-turning angle with nonuniform exit flow as compared to the full-length nozzle which has a uniform, parallel exit flow but a lower initial throat-turning angle. This trend was previously alluded to in the lower curves of figure 20 where it was shown that there was a large increase in internal surface area with only a minor gain in gross thrust as the nozzle was fully expanded to free-stream ambient pressure. The lowest amount of wetted internal surface area for a required gross-thrust level is attained with a shortened SY nozzle, with the larger amount of internal turning at the nozzle throat giving the best performance at the higher values of gross thrust.

REFERENCES

1. Edwards, C. L. W.: A Forebody Design Technique for Highly Integrated Bottom-Mounted Scramjets With Application to a Hypersonic Research Airplane. NASA TM X-71971, 1974.

2. Kirkham, Frank S.; Cubbage, James M.; Vahl, Walter A.; and Small, William J.: Studies of Airframe - Propulsion-System Integration for Mach 6 Cruise Vehicles. NASA TN D-4128, 1967.

3. Johnston, P. J.; Cubbage, J. M.; and Weidner, J. P.: Studies of Engine-Airframe Integration on Hypersonic Aircraft. J. Aircr., vol. 8, no. 7, July 1971, pp. 495-501.

4. Small, William J.; Weidner, John P.; and Johnston, P. J.: Scramjet Nozzle Design and Analysis as Applied to a Highly Integrated Hypersonic Research Airplane. NASA TM X-71972, 1974.

5. Weidner, John P.: Propulsion/Airframe Integration Considerations for High Altitude Hypersonic Cruise Vehicles. AIAA Paper No. 80-0111, Jan. 1980.

6. Weidner, John P.: Conceptual Study of a Turbojet/Ramjet Inlet. NASA TM-80141, 1979.

7. Jackson, Robert J.; and Wang, Tennyson T.: Hypersonic Ramjet Experiment Project - Phase I. Computer Program Description Ramjet and Scramjet Cycle Performance. NASA CR-132454, 1974.

8. Banes, B.; McIntyre, R. W.; and Simms, J. A.: Properties of Air and Combustion Products With Kerosine and Hydrogen Fuels, Volume VIII - Thermodynamic Properties for Fuel-Weak Mixtures: Hydrogen/Air. AGARD, 1967. Volume XI - Thermodynamic Properties for Stoichiometric and Fuel-Rich Mixtures: Hydrogen/Air. AGARD, 1967.

9. Salas, Manuel D.: Shock Fitting Method for Complicated Two-Dimensional Supersonic Flows. AIAA J., vol. 14, no. 5, May 1976, pp. 583-588.

10. Salas, Manuel D.: The Numerical Calculation of Inviscid Plume Flow Fields. AIAA Paper No. 74-523, June 1974.

11. Ames Research Staff: Equations, Tables, and Charts for Compressible Flow. NACA Rep. 1135, 1953.

12. Shapiro, Ascher H.: The Dynamics and Thermodynamics of Compressible Fluid Flow, Vol. I. Ronald Press Co., c.1953.

13. Crown, J. Conrad: Supersonic Nozzle Design. NACA TN 1651, 1948.

Table I.- BASELINE VALUES ASSUMED FOR CRUISE-RANGE CALCULATIONS

Gross takeoff mass (with nominal inlet and exhaust nozzle), kg	90 718
Sea-level thrust loading	0.48
Turbojet thrust/weight (includes inlet requirements)	6
Total fuel capacity, kg	24 494
Fuel to accelerate to cruise (percent of gross takeoff mass)	10
Nominal total inlet area (turbojet and ramjet), m^2	9.29
Fuel equivalence ratio at cruise	0.6
Ramjet mass (includes inlet requirements; based on total inlet area), kg/m^2	1171.78
Exhaust nozzle mass (based on internal surface area), kg/m^2	48.82
Mass at end of cruise (with nominal inlet and exhaust nozzle), kg	66 224

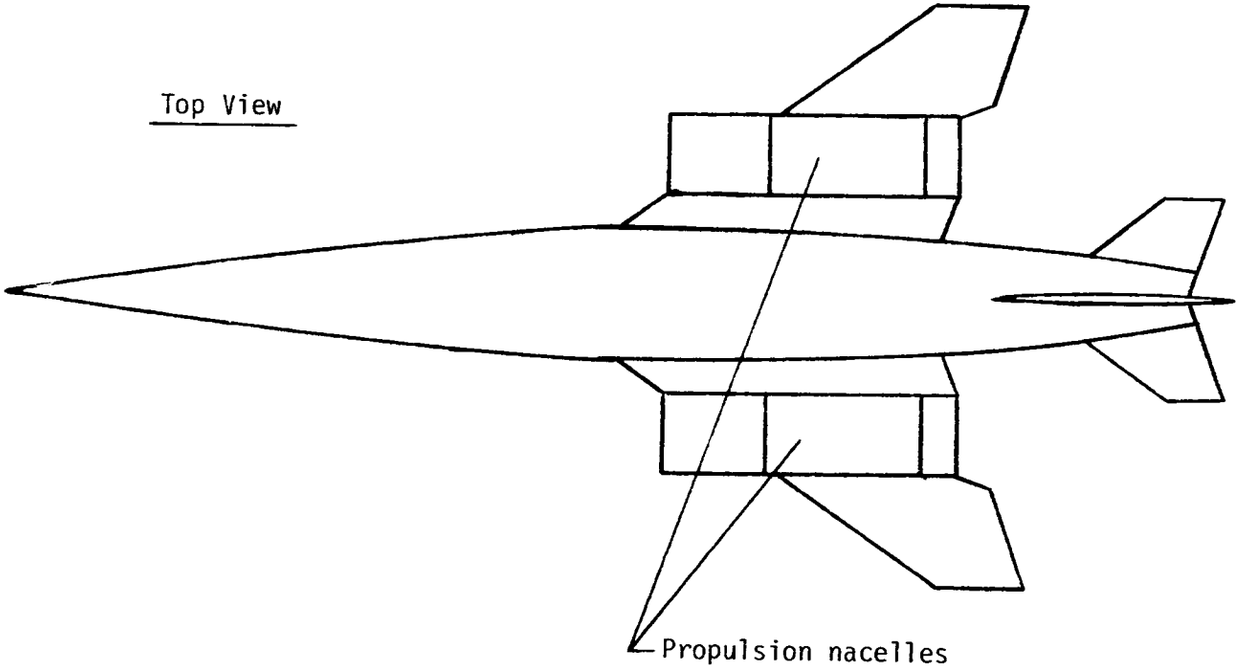

Figure 1.- Typical hypersonic-cruise-vehicle concept with top-mounted ramjet-propulsion nacelles.

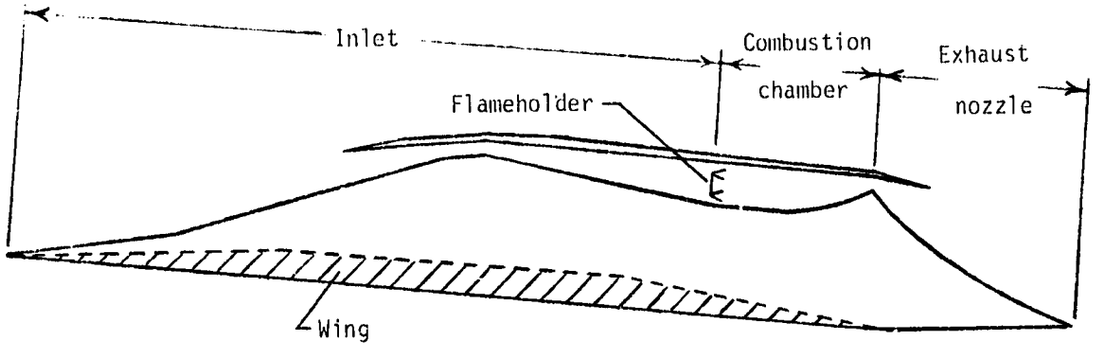

Asymmetric inverted (AI) nozzle

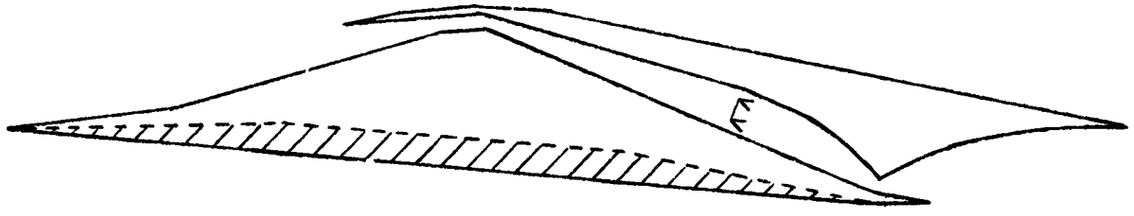

Asymmetric upright (AU) nozzle

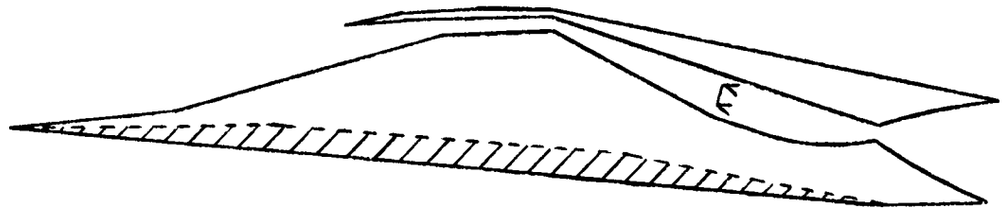

Symmetric (SY) nozzle

Figure 2.- Nozzle/nacelle configurations.

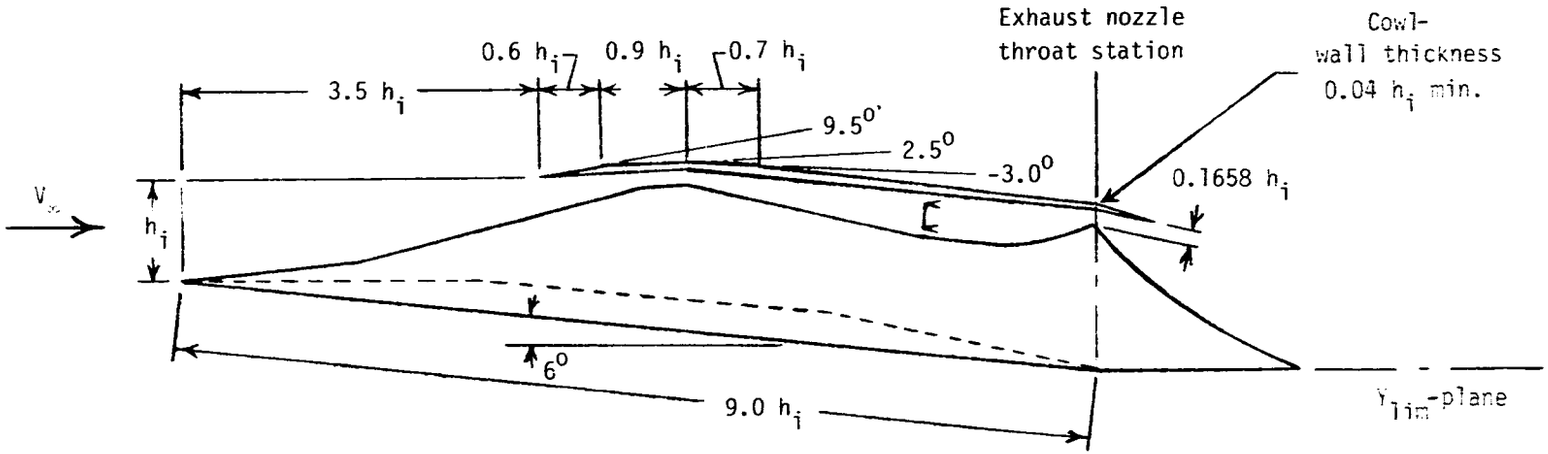

Figure 3.- Nacelle geometry of AI nozzle.

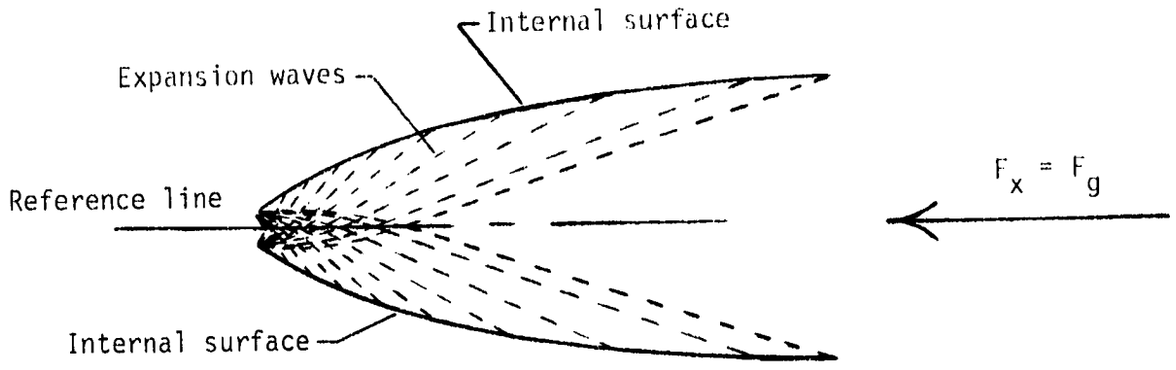

Symmetric (SY) nozzle

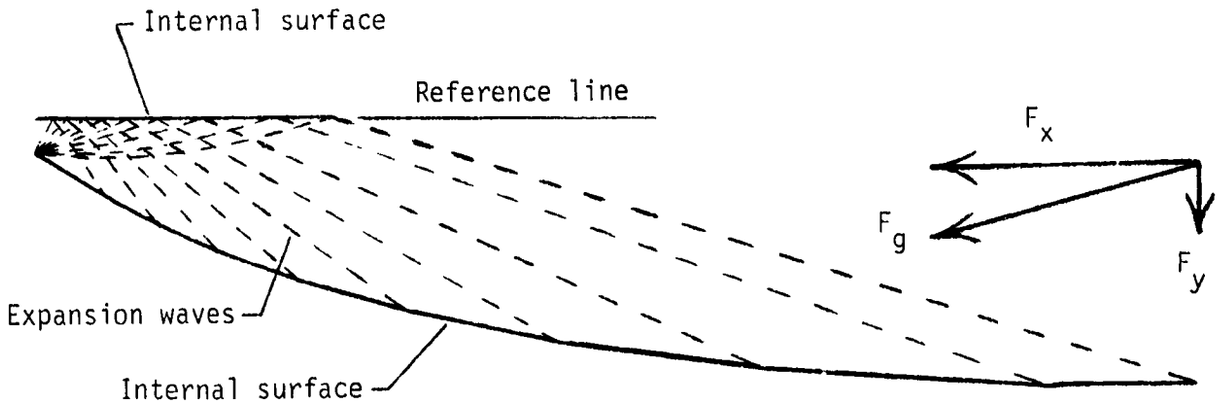

Asymmetric inverted (AI) nozzle

Figure 4.- Types of two-dimensional isentropic nozzles.

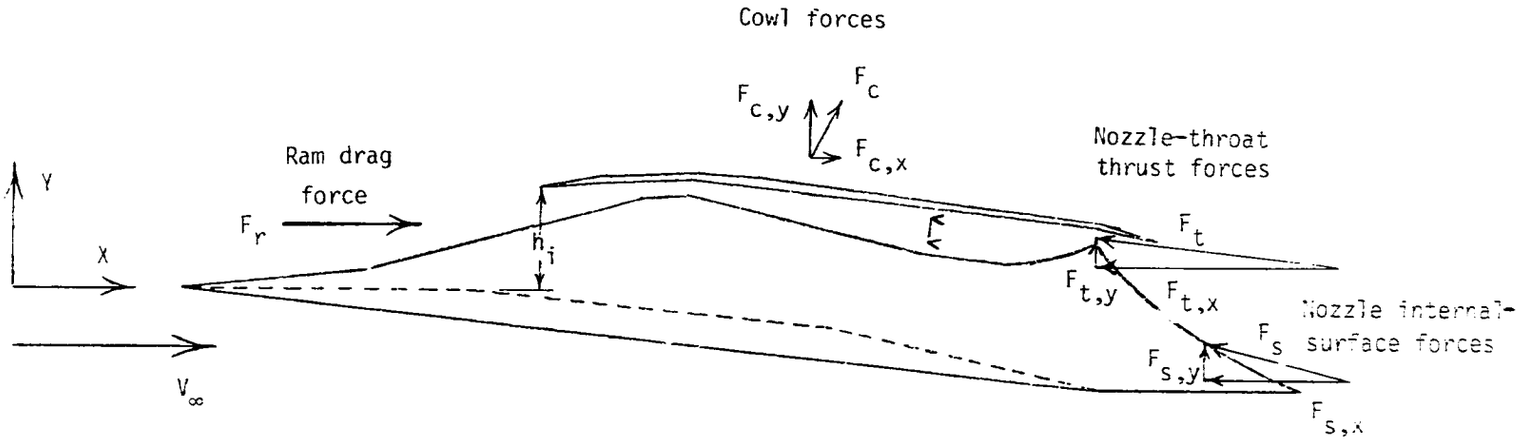

$$F_r = \rho_\infty A_i V_\infty^2 + (p_\infty - p_\infty) A_i \quad (0)$$

$$F_t = \rho_t A_t V_t^2 + (p_t - p_\infty) A_t$$

$$F_c = \int_{\text{Cowl surface}} (p - p_\infty)\, dA$$

$$F_s = \int_{\text{Nozzle surface}} (p - p_\infty)\, dA$$

Gross thrust $\quad F_g = F_t + F_s$

Net lift $\quad F_L = F_{t,y} + F_{s,y} + F_{c,y}$

Net propulsive thrust $\quad F_v = F_{t,x} + F_{s,x} + F_{c,x} - F_r$

Propulsive $\quad I_{sp} = F_v / \dot{m}$

Figure 5.- Nacelle force accounting.

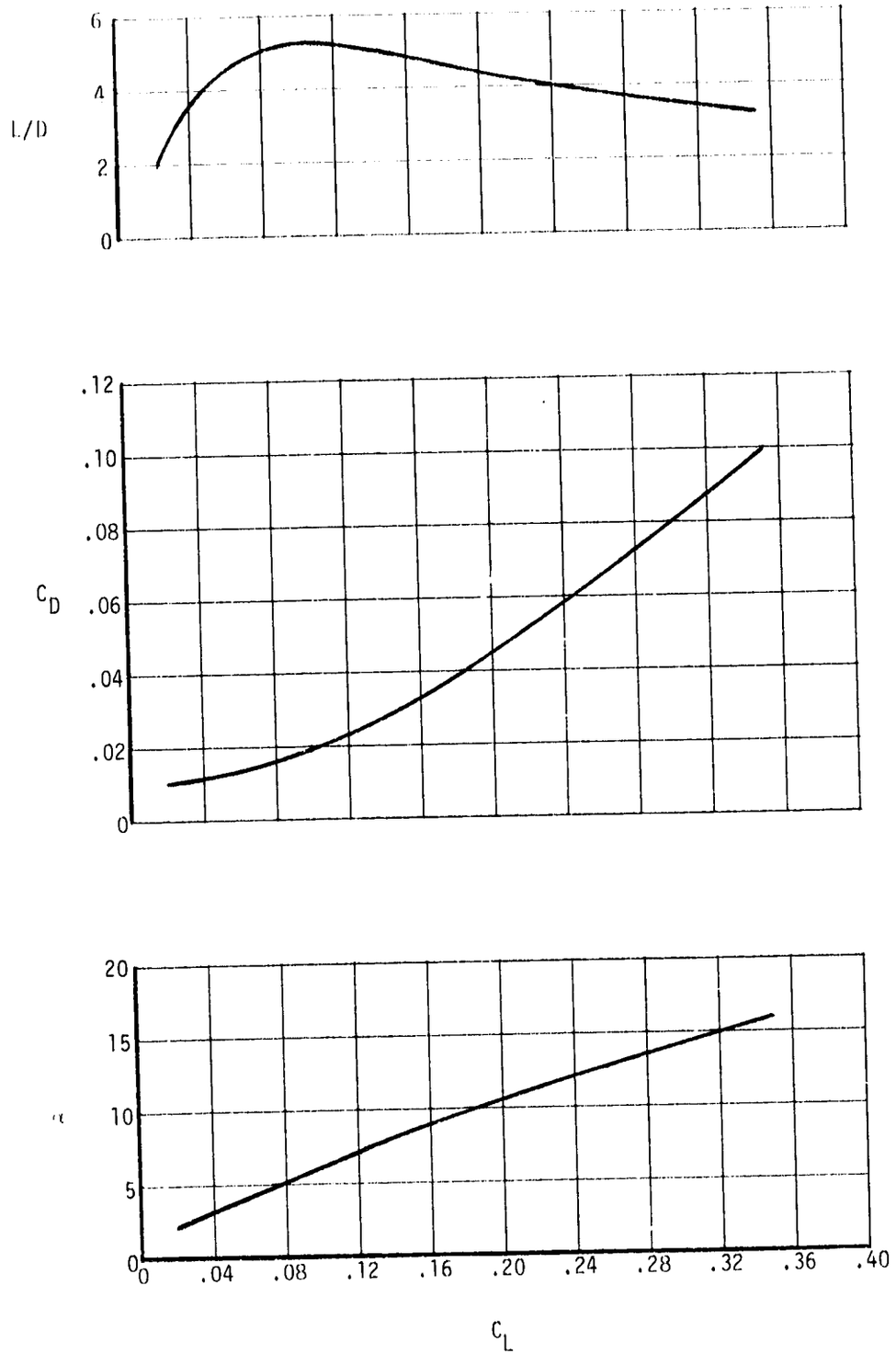

Figure 6.- Representative hypersonic-cruise-vehicle aerodynamics at Mach 5.

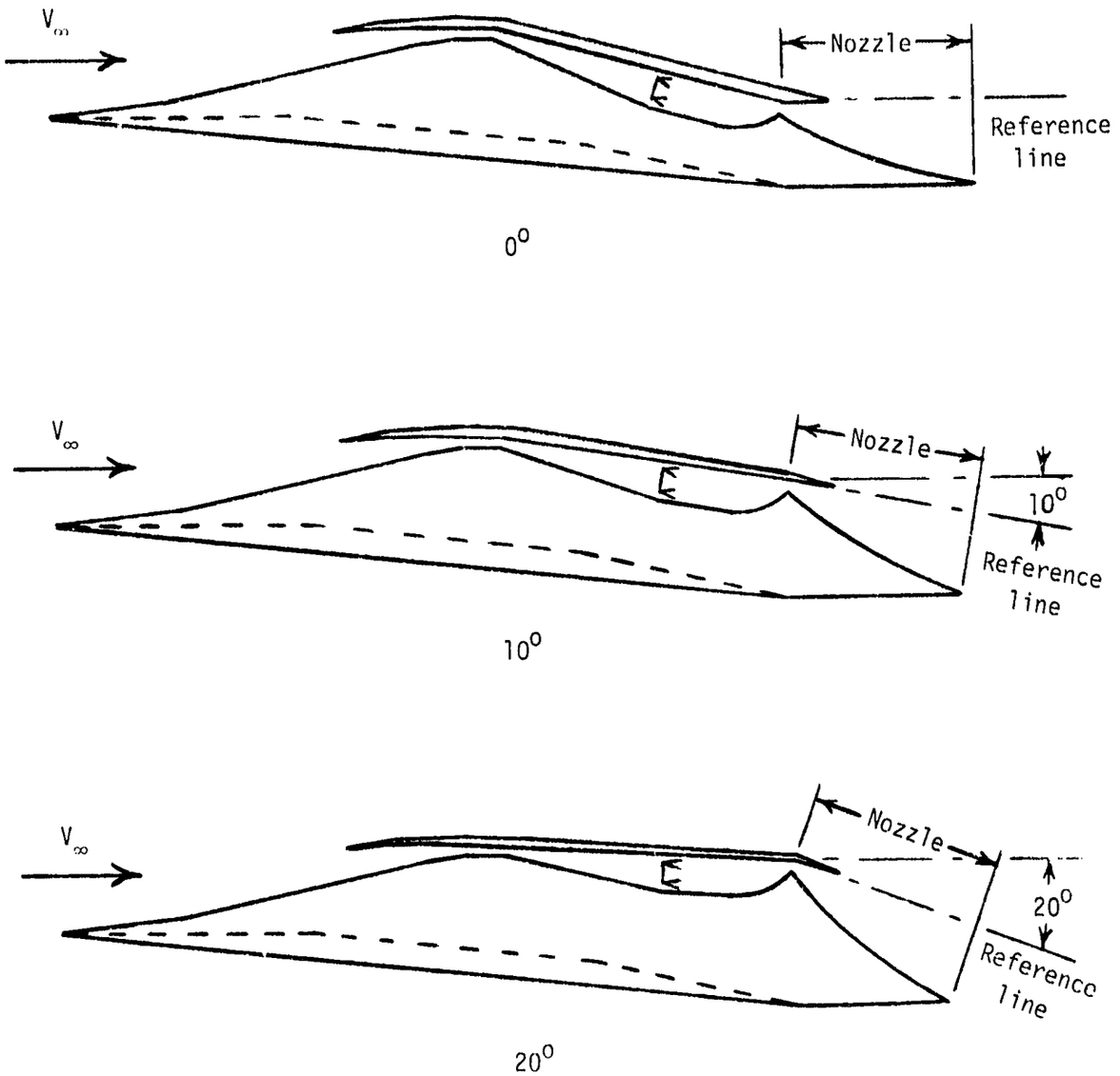

Figure 7.- Nacelle with typical AI nozzle orientation at 0°, 10°, and 20° relative to free-stream direction.

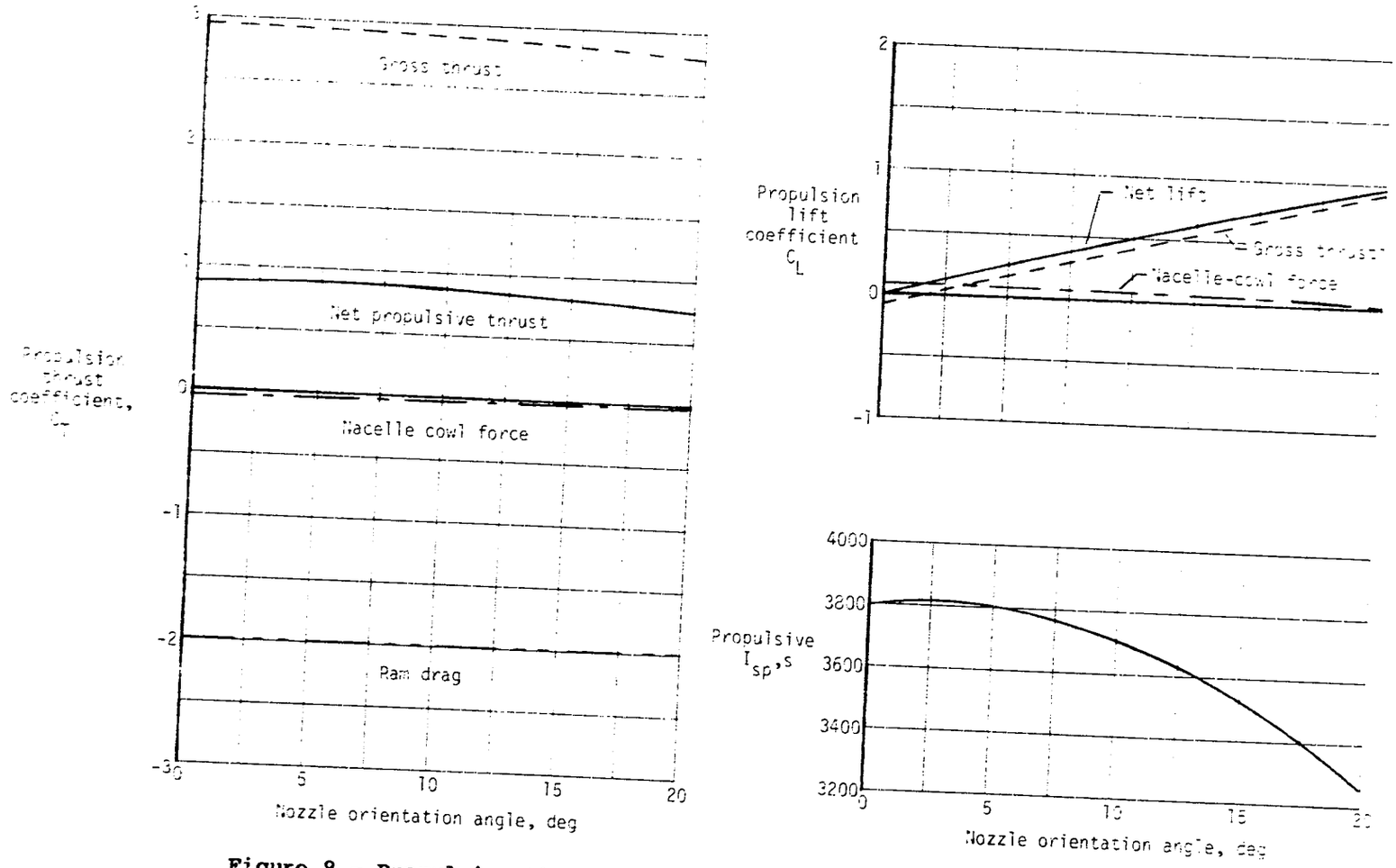

Figure 8.- Propulsion thrust and lift forces for typical AI nozzle.

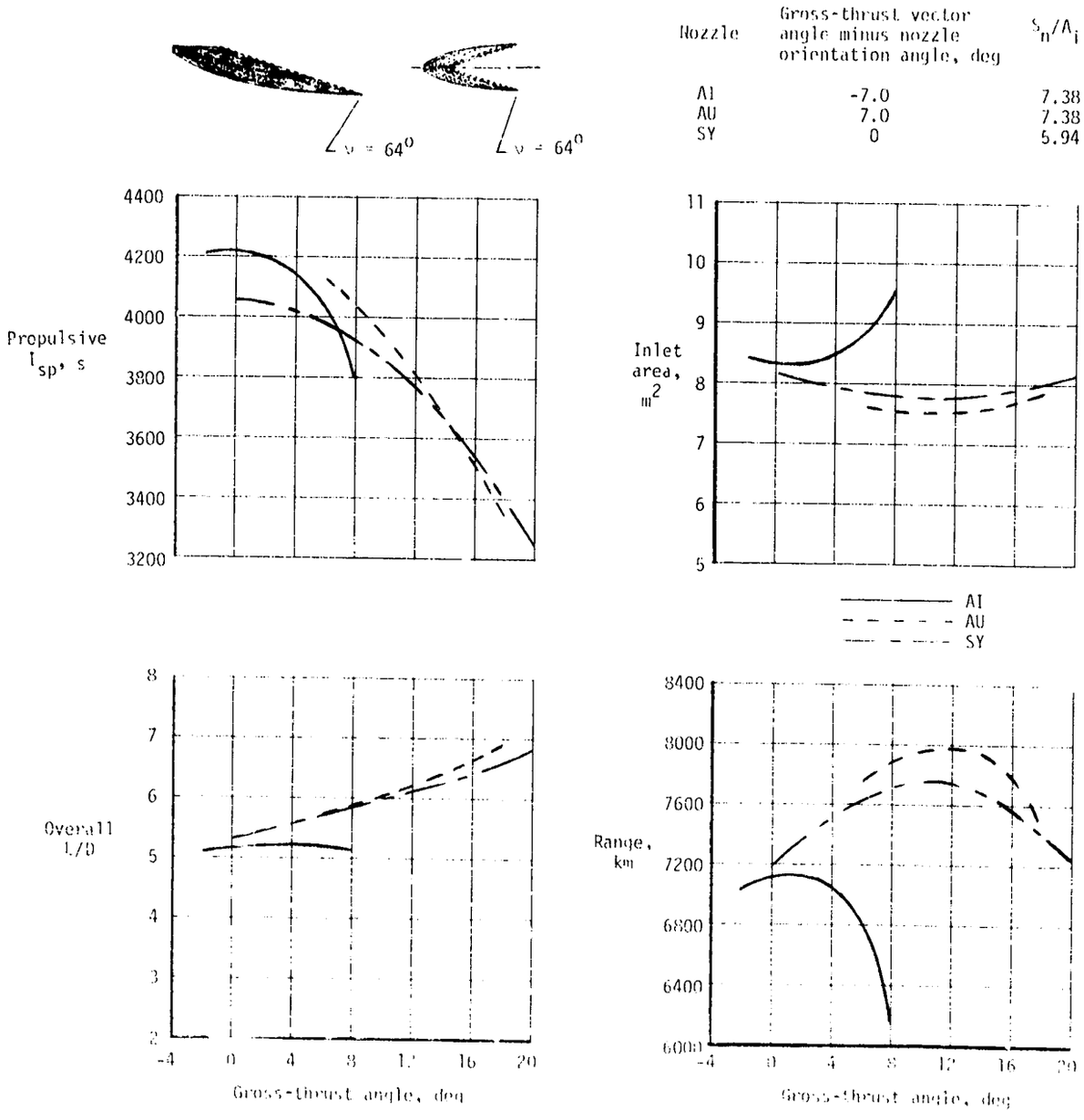

(a) Full-length nozzles, $\nu = 64^{\circ}$.

Figure 9.- Cruise-range performance of 64° turning full-length and shortened nozzles.

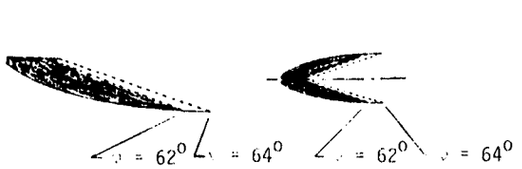

Nozzle	Gross-thrust vector angle minus nozzle orientation angle, deg	A_n/A_i
AI	-5.9	6.19
AU	5.9	6.19
SY	0	5.04

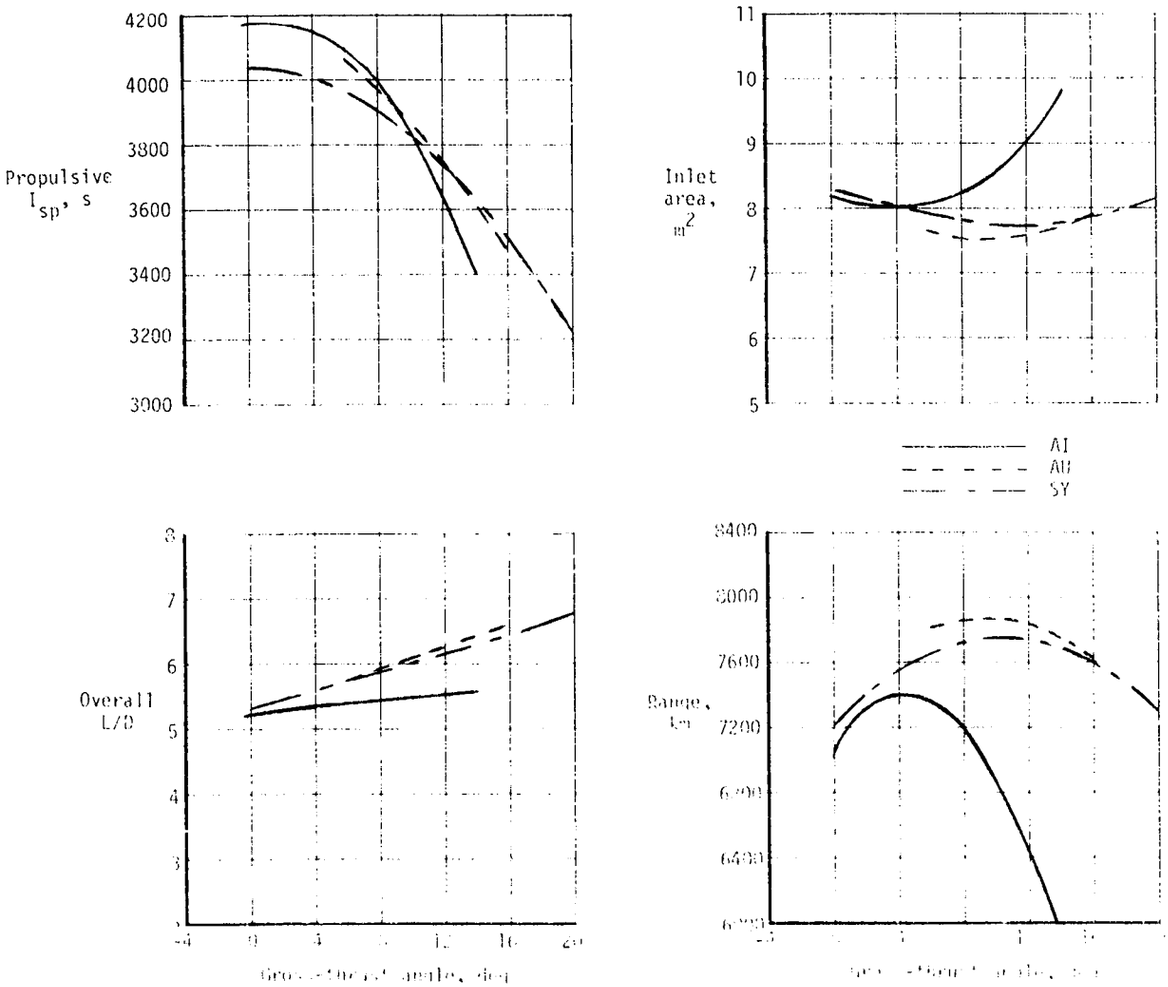

(b) Shortened nozzles, $\nu = 62^{\circ}$.

Figure 9.- Continued.

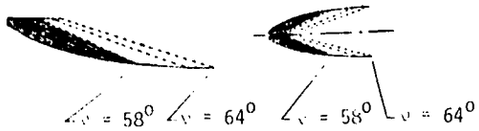

Nozzle	Gross-thrust vector angle minus nozzle orientation angle, deg	S_n/A_i
AI	-3.7	4.48
AU	3.7	4.48
SY	0	3.68

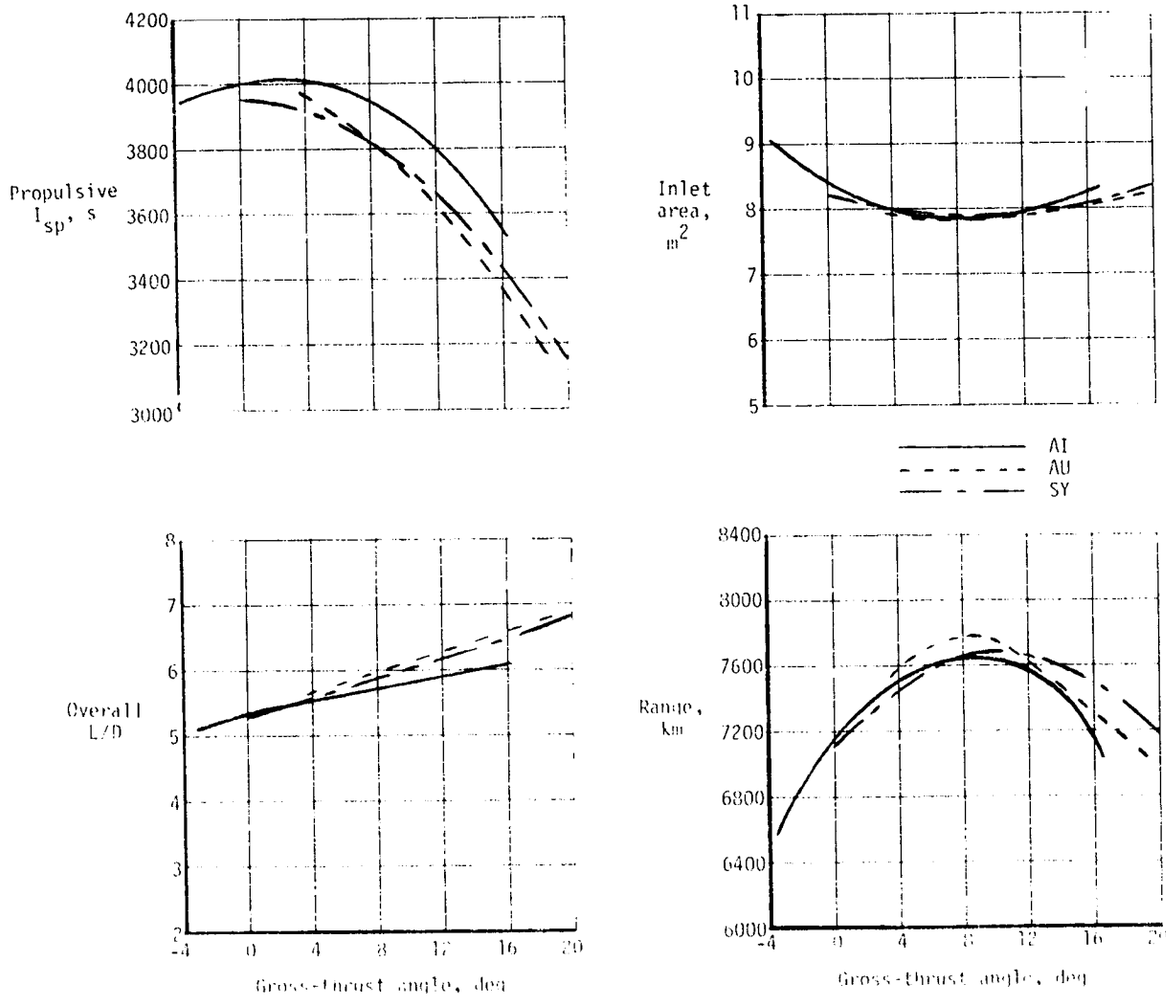

(c) Shortened nozzles, ν = 58°.

Figure 9.- Continued.

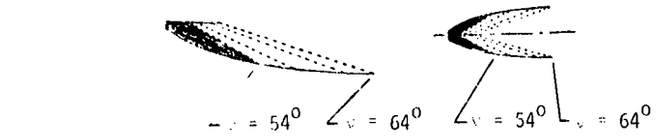

Nozzle	Gross-thrust vector angle minus nozzle orientation angle, deg	S_n/A_i
AI	-1.5	3.27
AU	1.5	3.27
SY	0	2.68

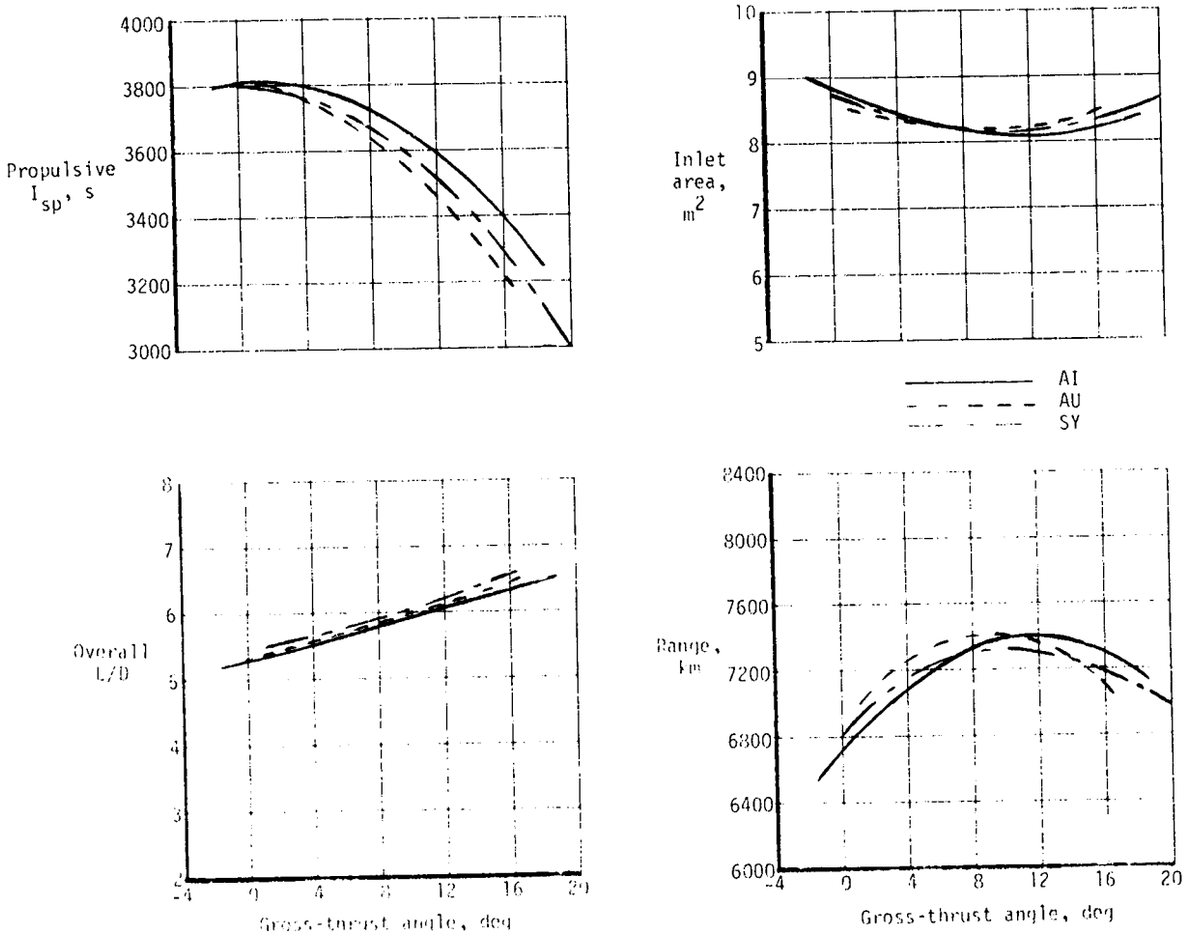

(d) Shortened nozzles, $\nu = 54^{\circ}$.

Figure 9.- Continued.

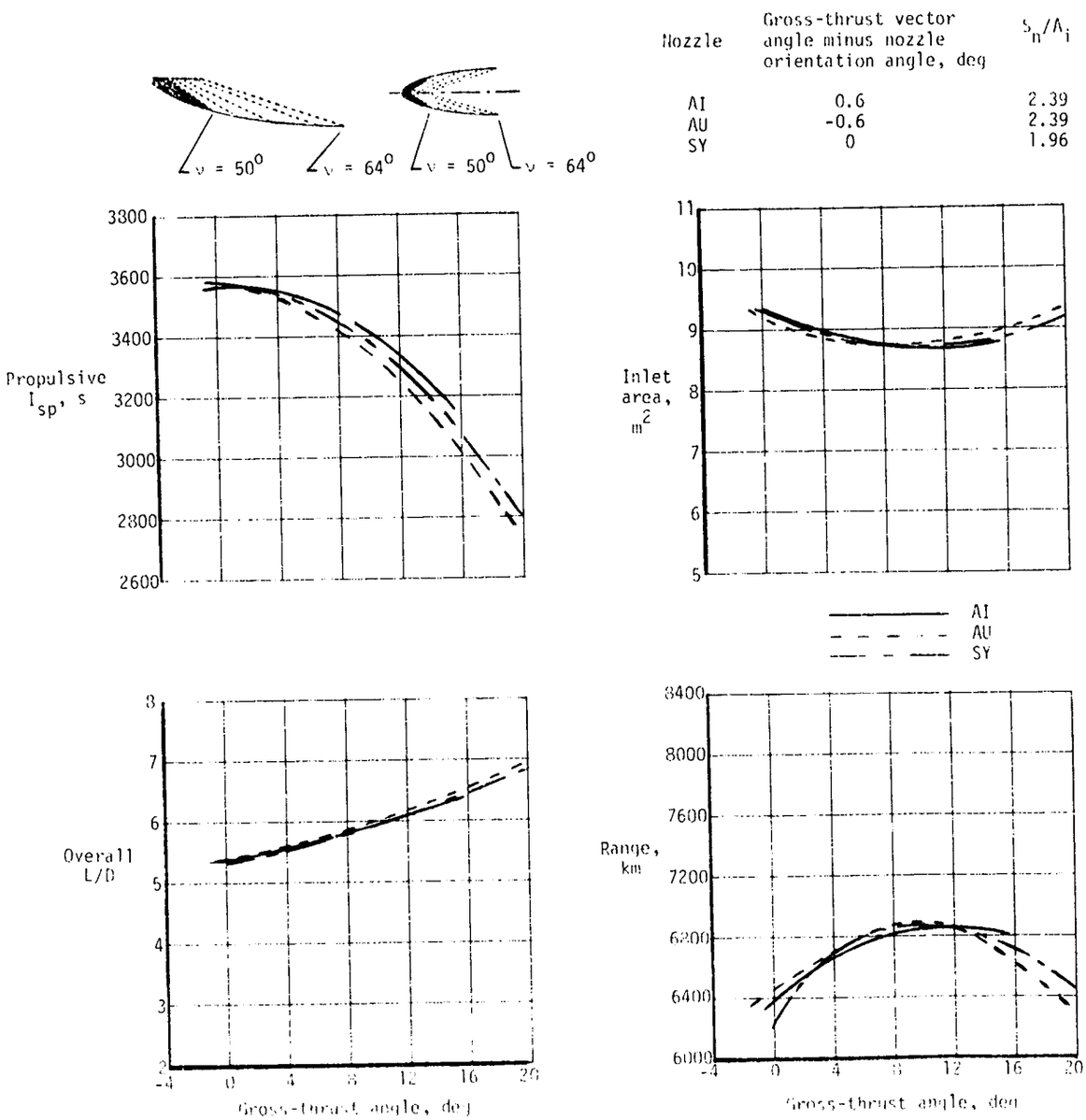

(e) Shortened nozzles, $\nu = 50^{o}$.

Figure 9.- Continued.

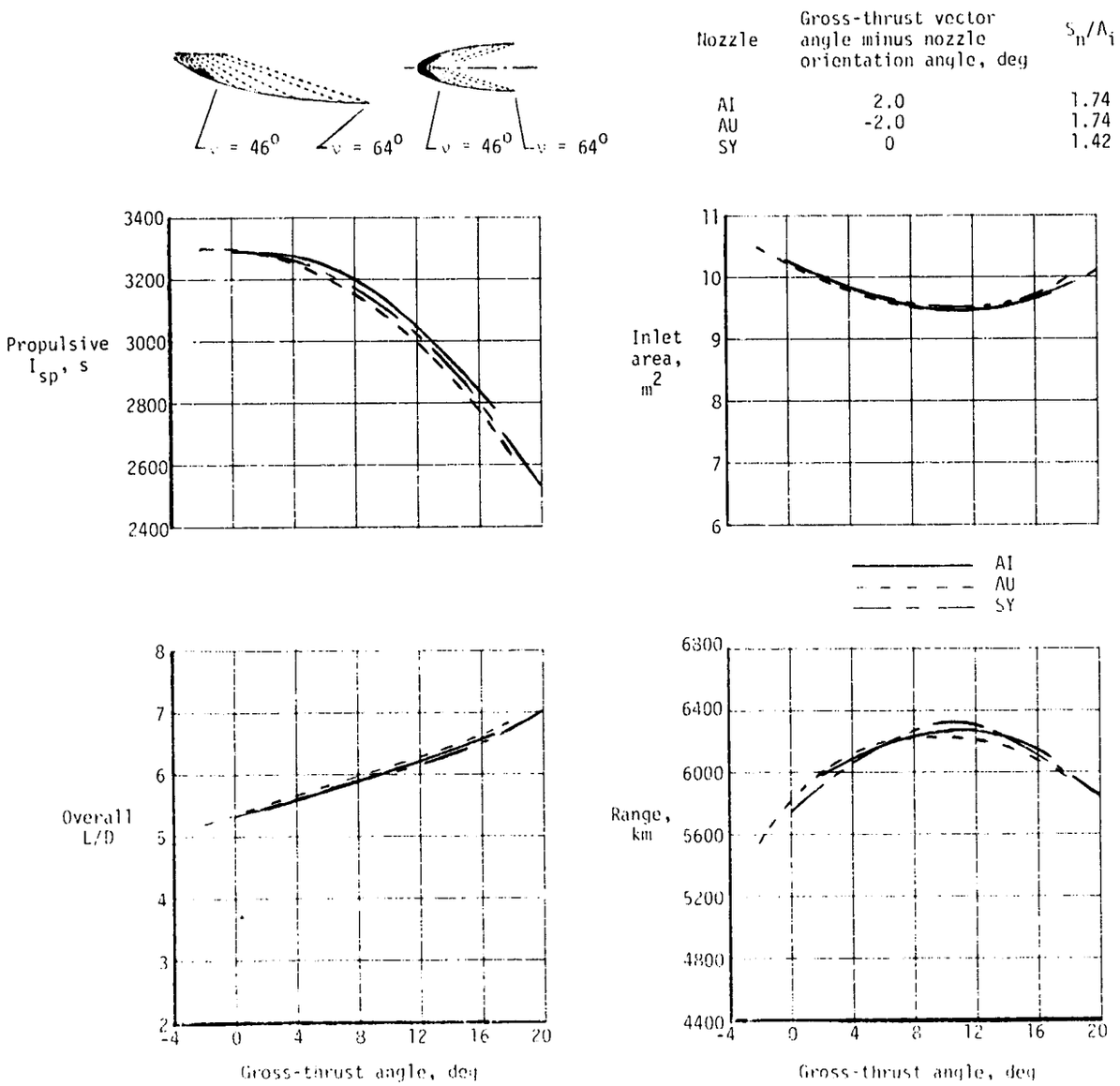

(f) Shortened nozzles, $\nu = 46^{\circ}$.

Figure 9.- Continued.

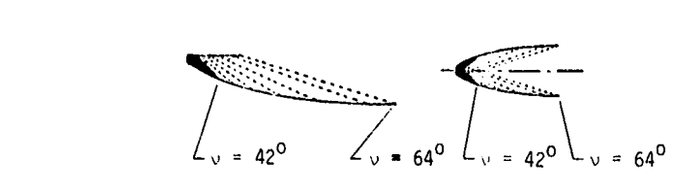

Nozzle	Gross-thrust vector angle minus nozzle orientation angle, deg	S_n/A_i
AI	3.3	1.27
AU	-3.3	1.27
SY	0	1.03

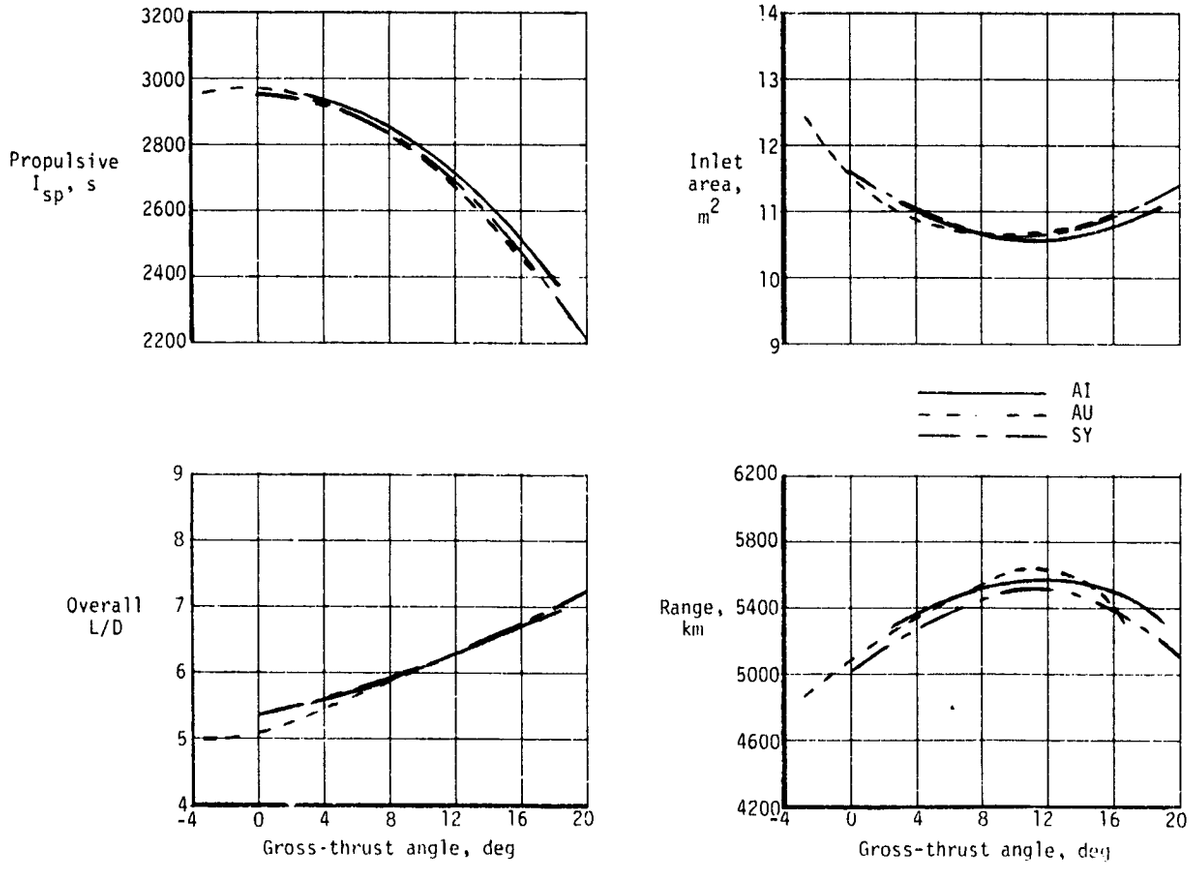

(g) Shortened nozzles, $\nu = 42^{\circ}$.

Figure 9.- Concluded.

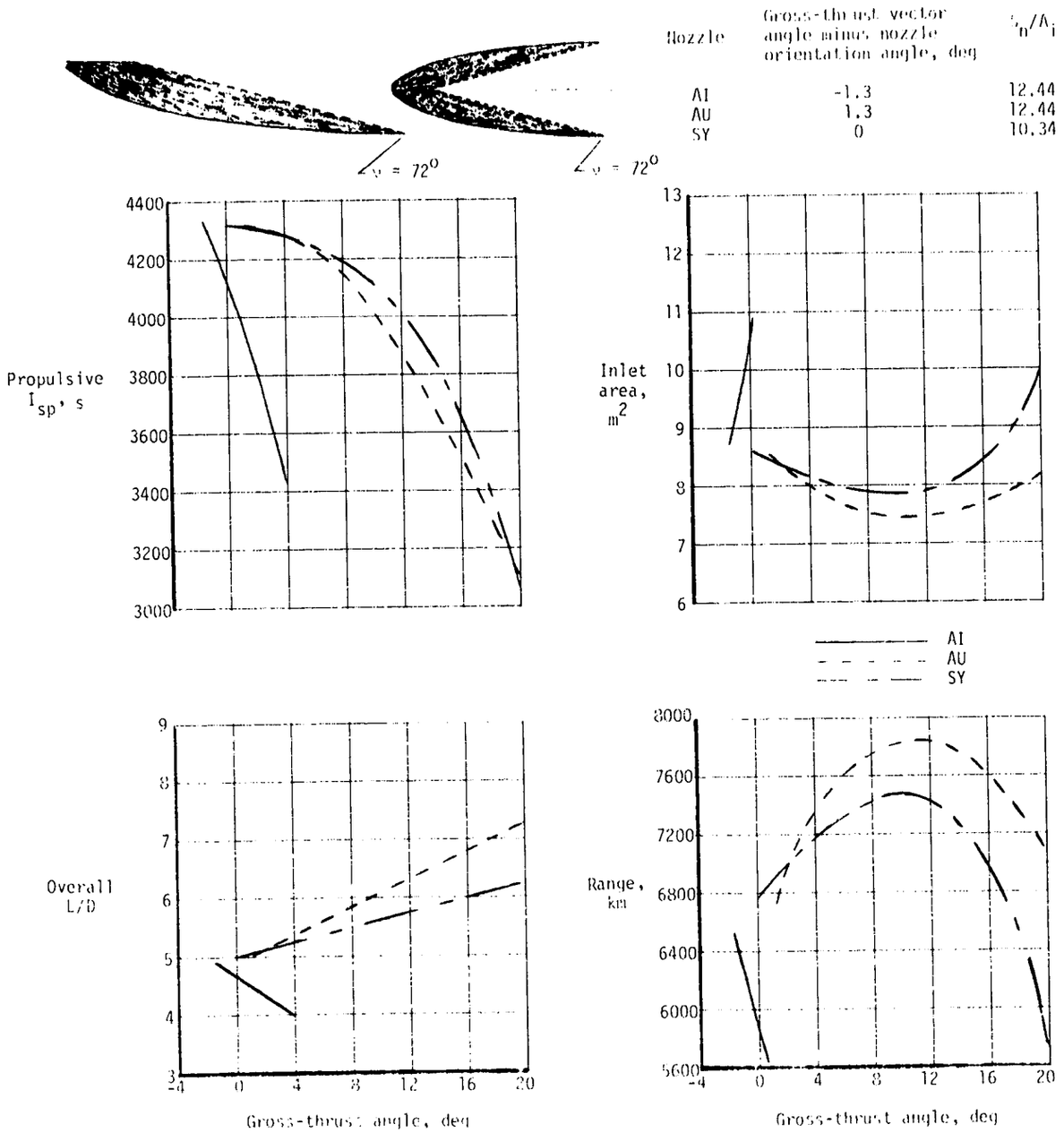

(a) Full-length nozzles, $\nu = 72^{\circ}$.

Figure 10.- Cruise-range performance of 72° turning full-length and shortened nozzles.

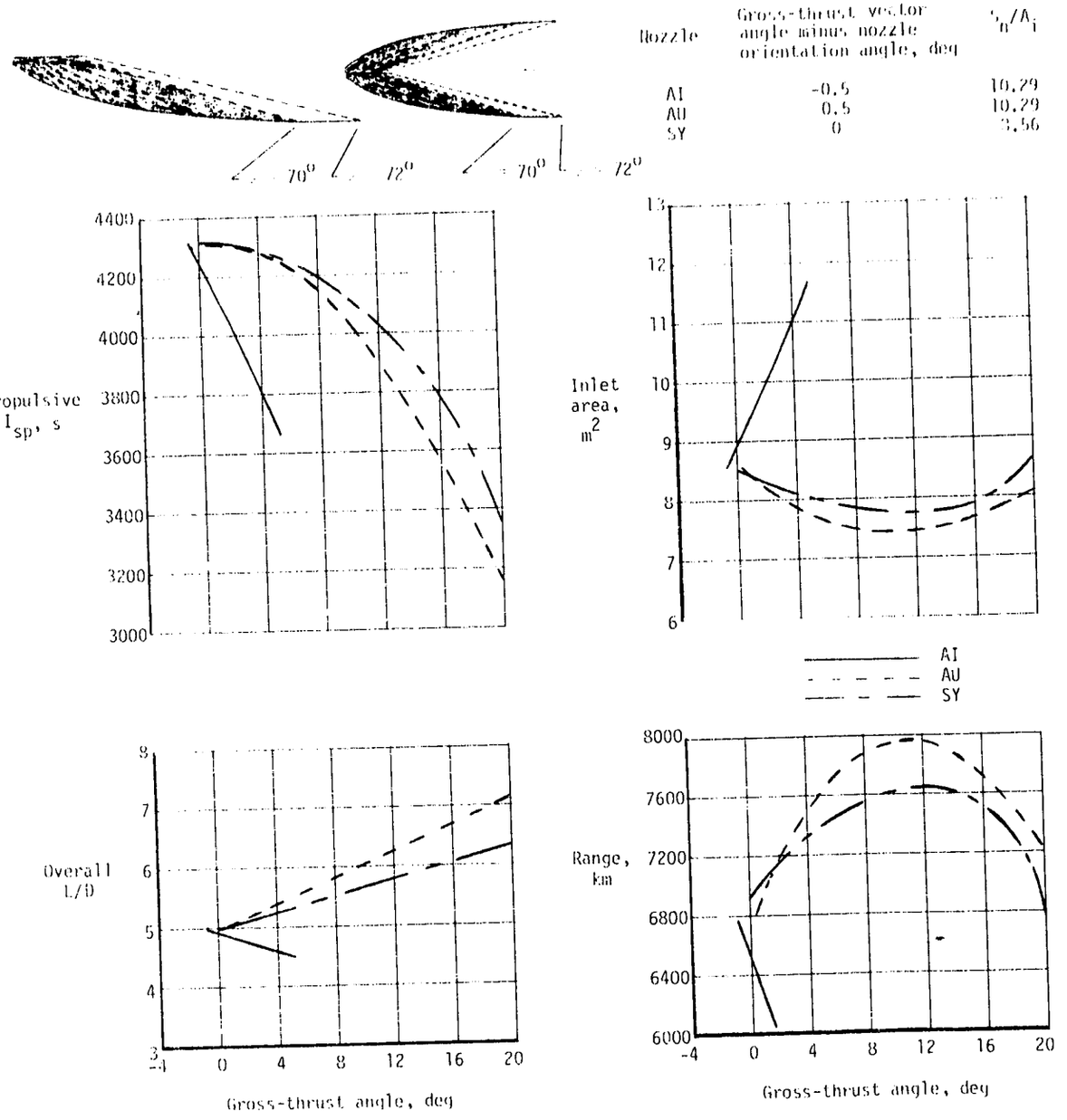

(b) Shortened nozzles, $\nu = 70^{\circ}$.

Figure 10.- Continued.

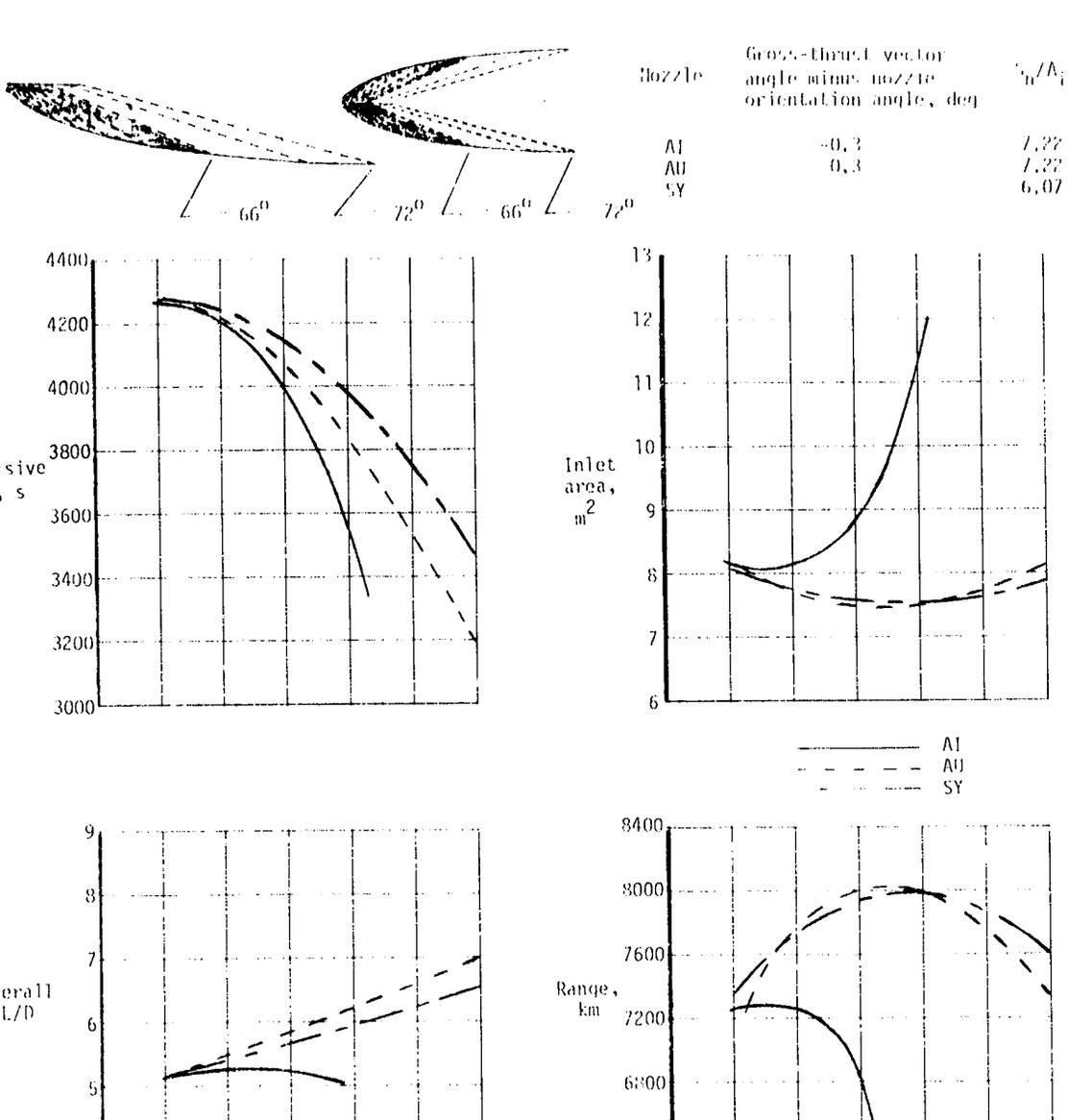

(c) Shortened nozzles, $\nu = 66^{\circ}$.

Figure 10.- Continued.

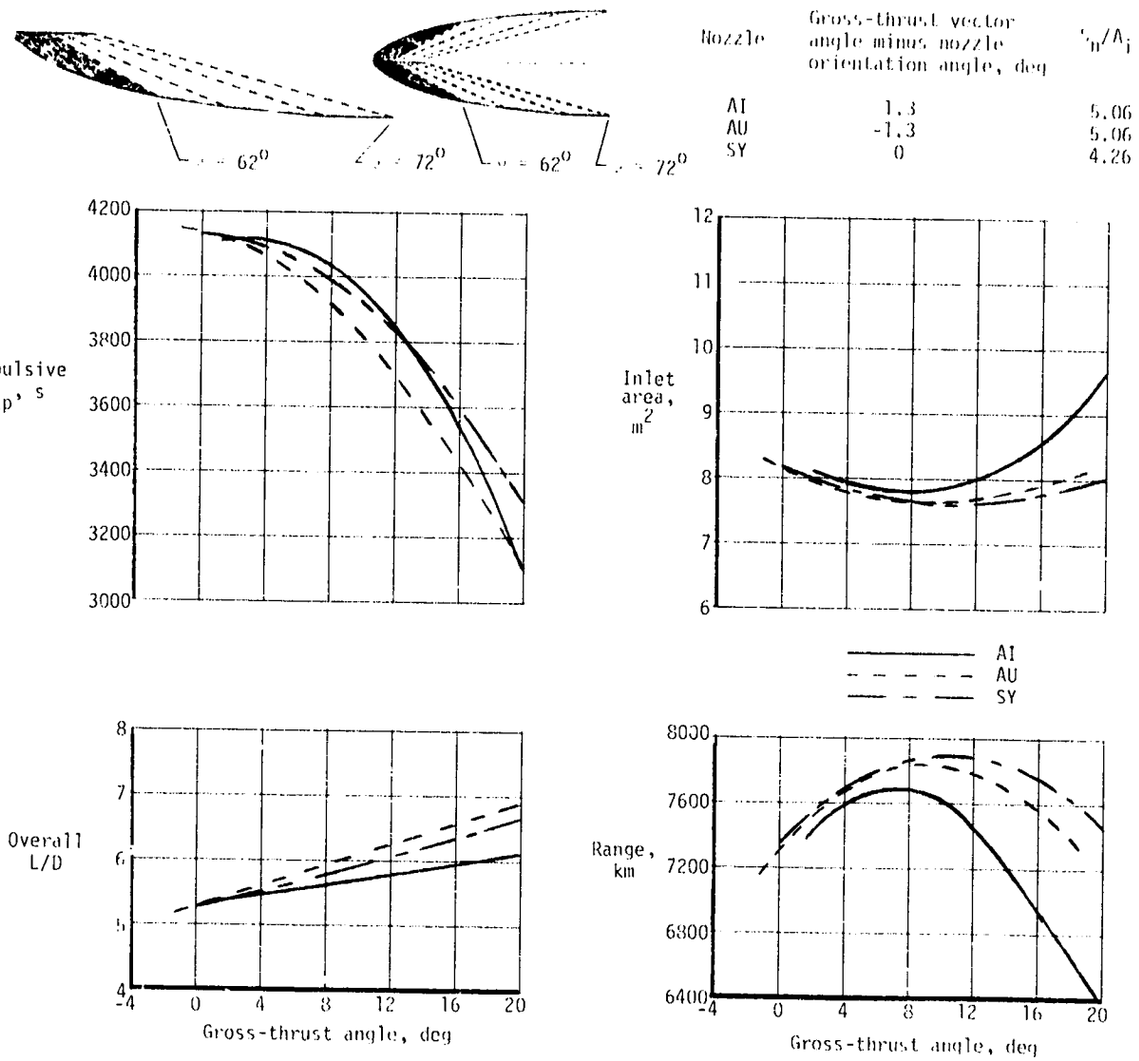

(d) Shortened nozzles, $\nu = 62^{\circ}$.

Figure 10.- Continued.

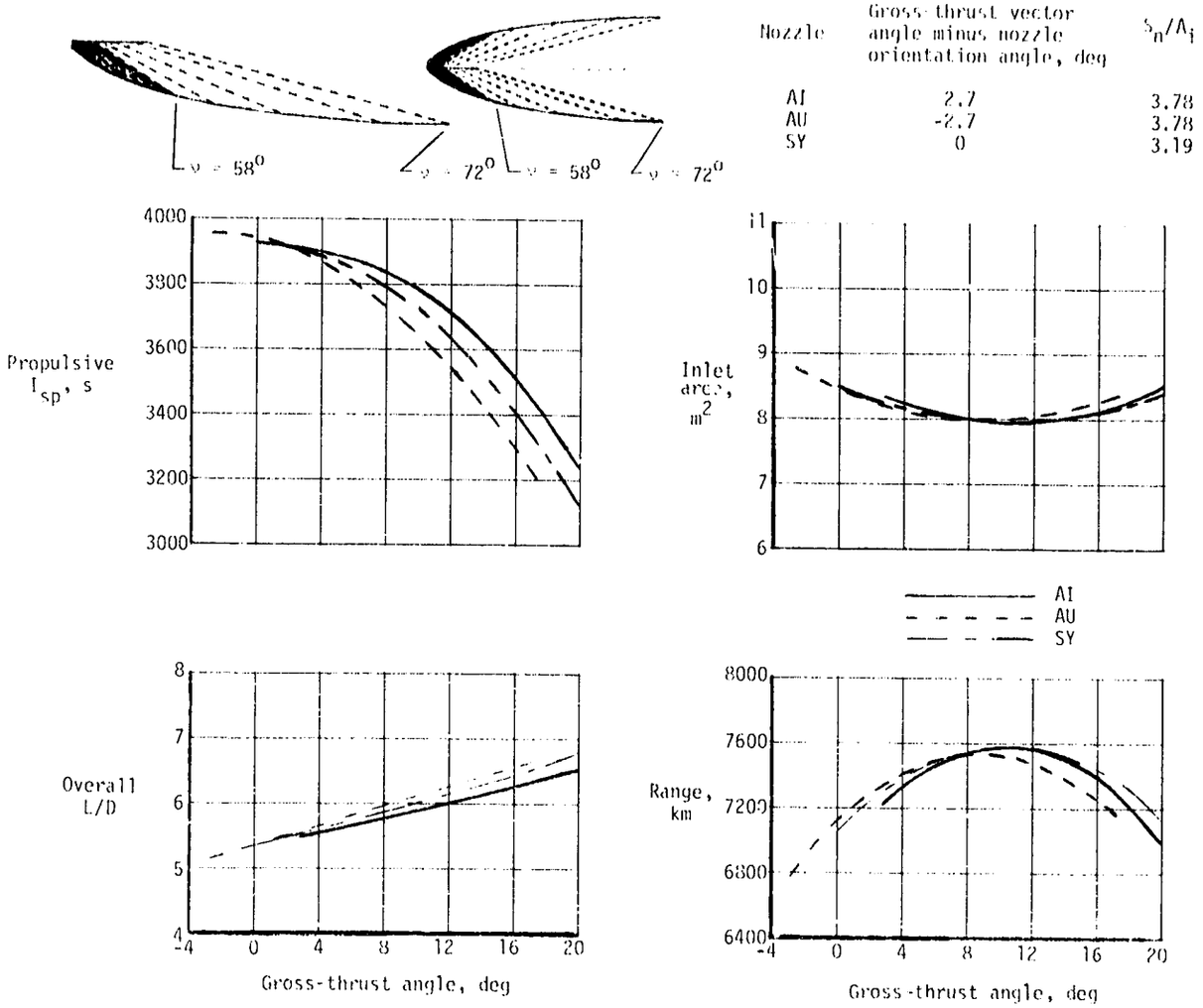

(e) Shortened nozzles, $\nu = 58^{o}$.

Figure 10.- Continued.

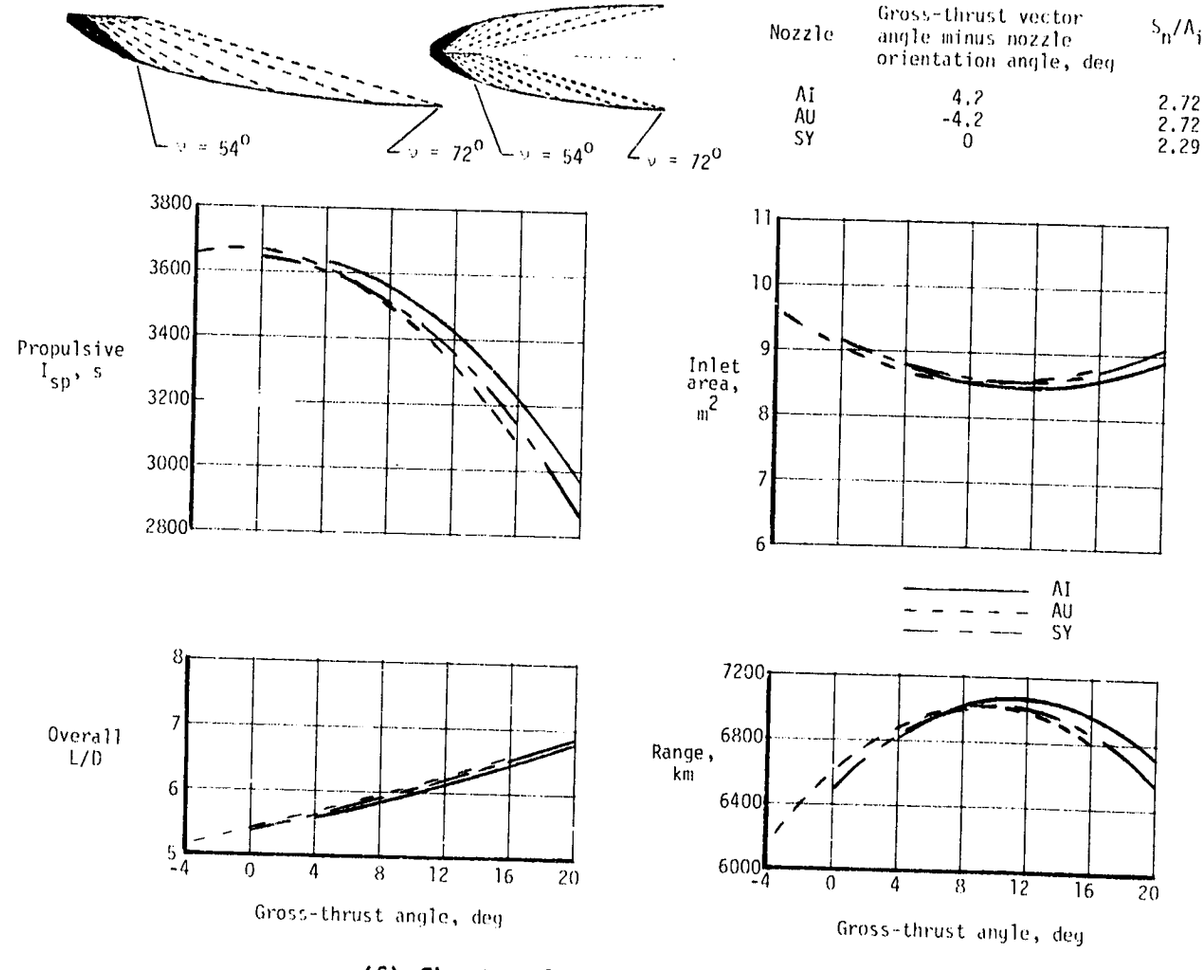

(f) Shortened nozzles, $\nu = 54^{o}$.

Figure 10.- Continued.

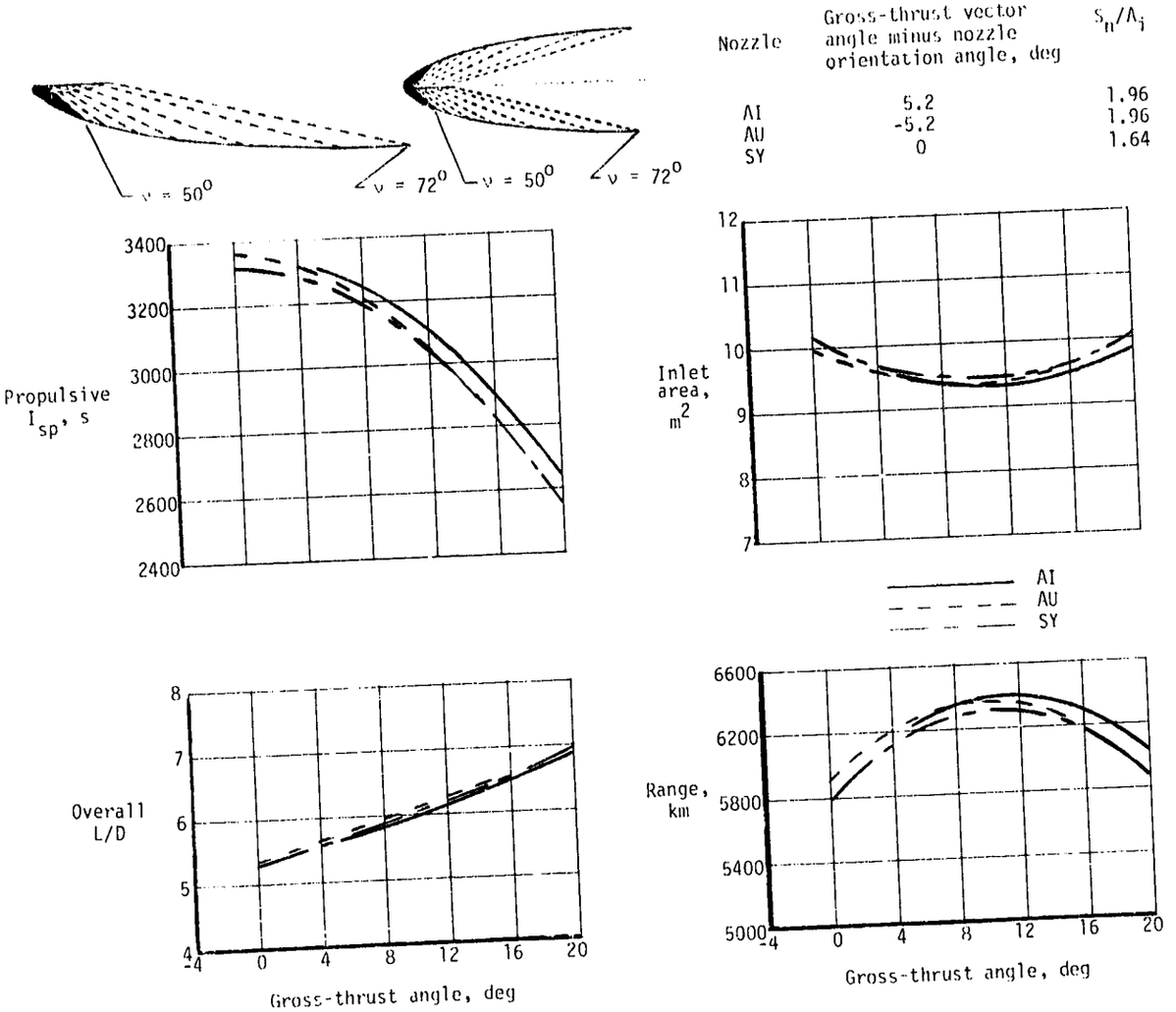

(g) Shortened nozzles, $\nu = 50^{o}$.

Figure 10.- Continued.

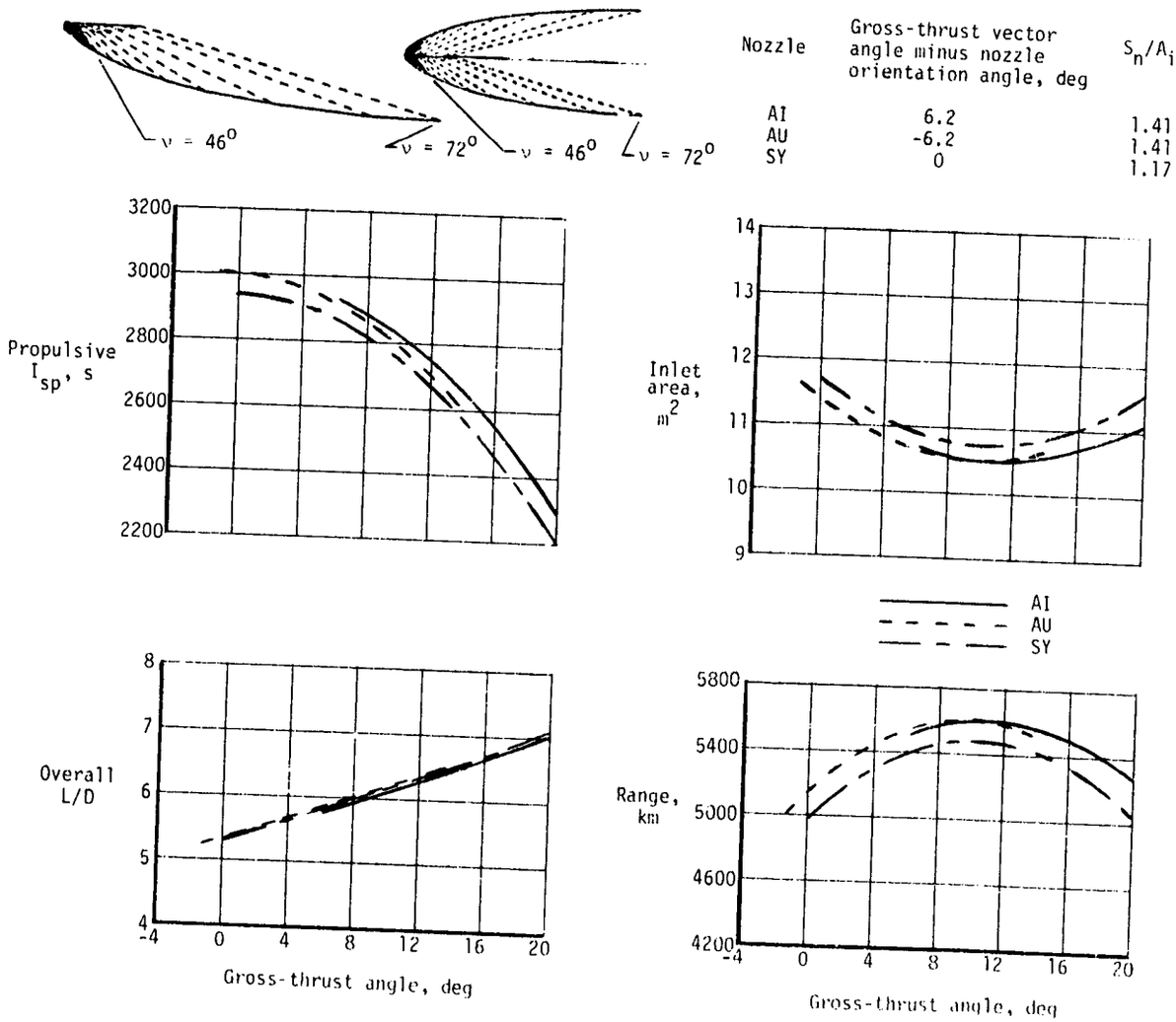

(h) Shortened nozzles, $\nu = 46°$.

Figure 10.- Concluded.

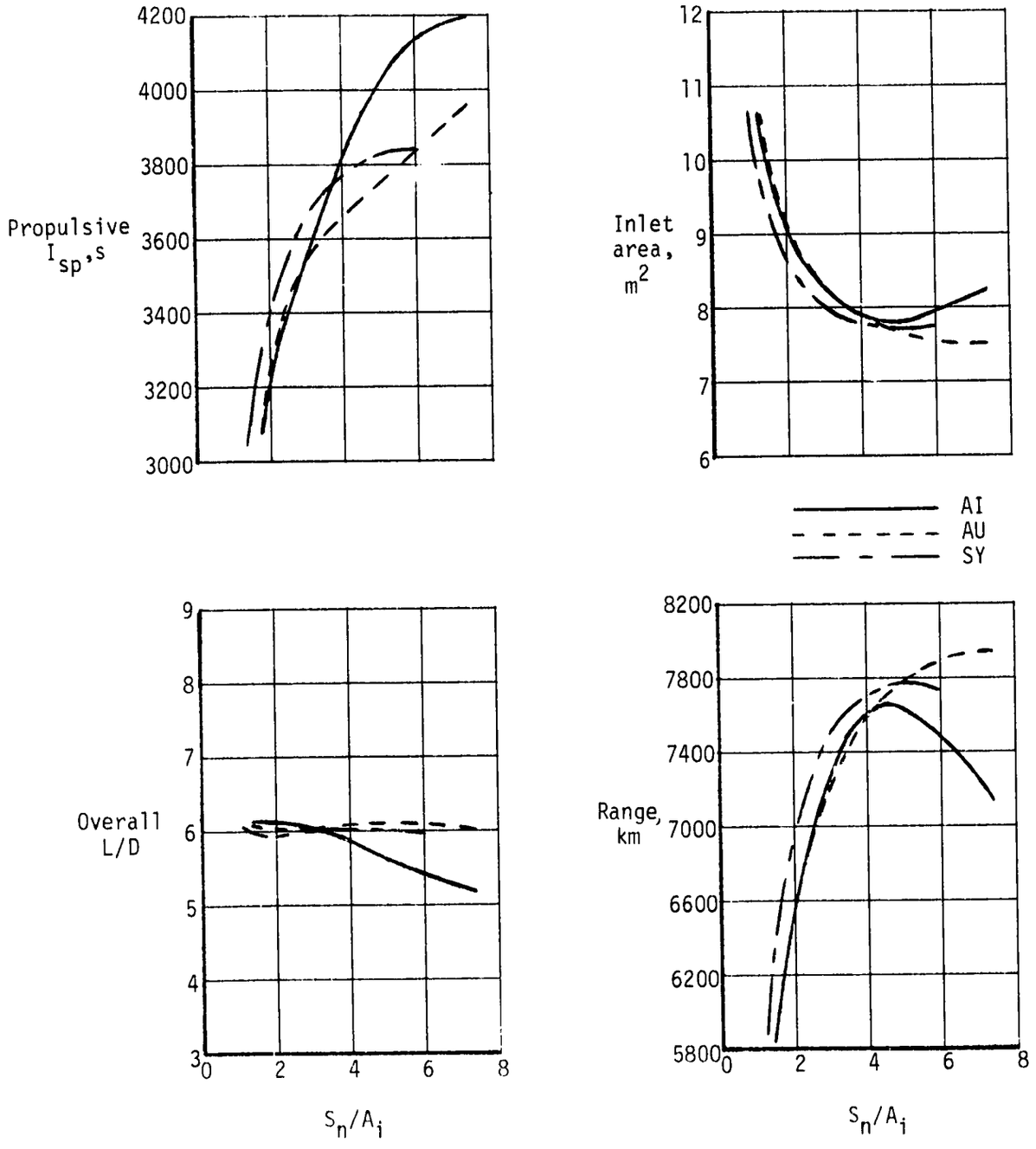

(a) $\nu = 64^{o}$; full-length and shortened nozzles.

Figure 11.- Cruise-range performance of optimum nozzle installations.

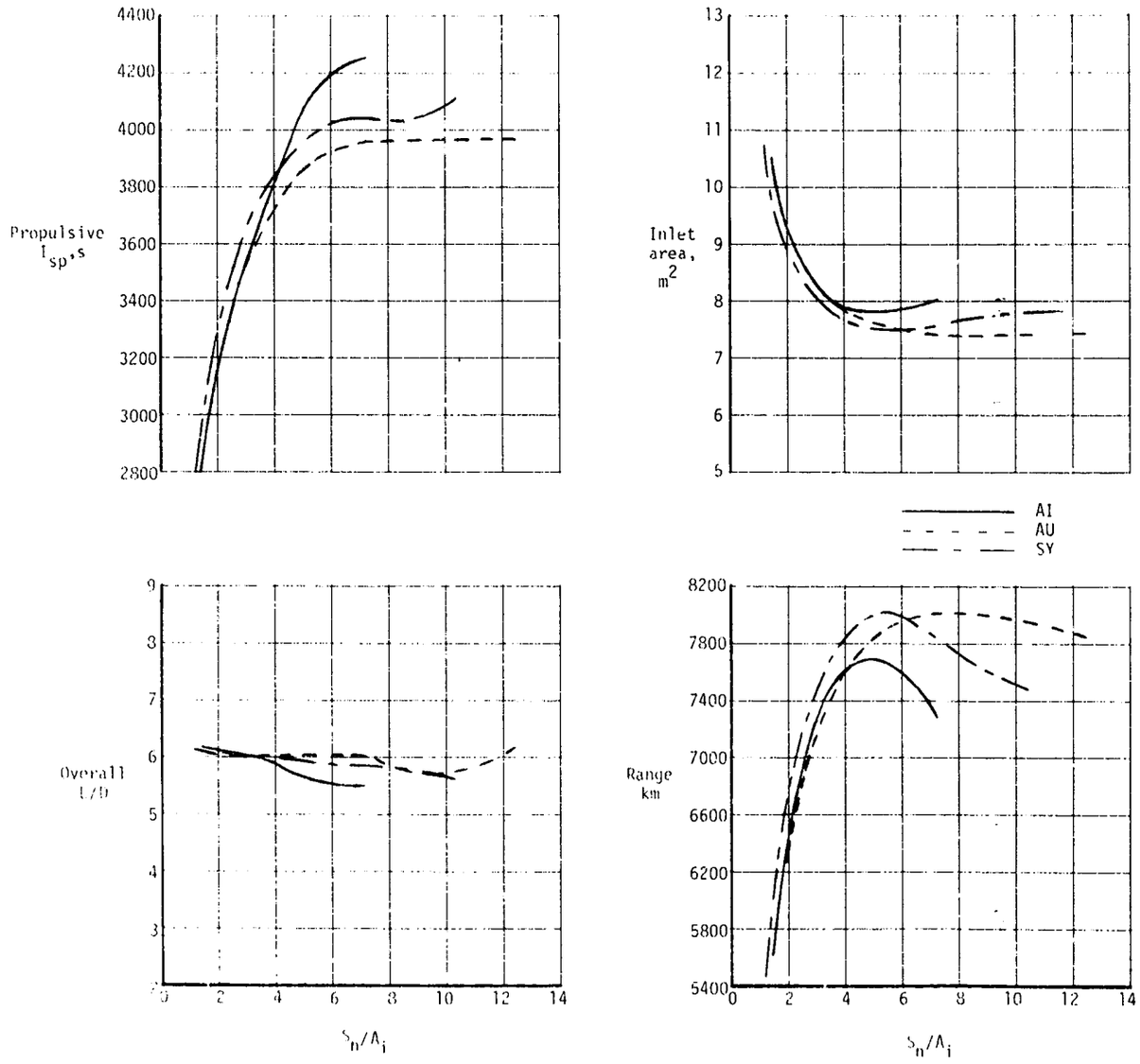

(b) $\nu = 72^{o}$; full-length and shortened nozzles.

Figure 11.- Concluded.

Nozzle	Orientation angle, deg	Gross-thrust angle, deg	S_n/A_j
AI	6.0	7.6	5.0
AU	10.0	10.0	7.2
SY	11.2	11.2	5.3

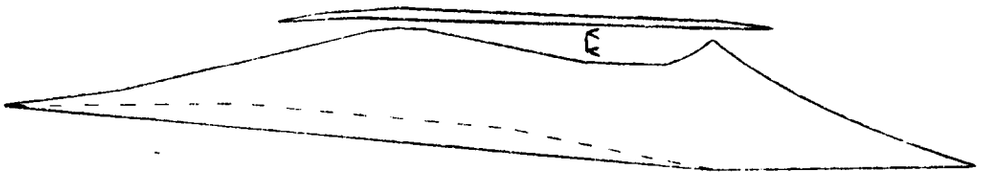

AI nozzle, ν = 61°

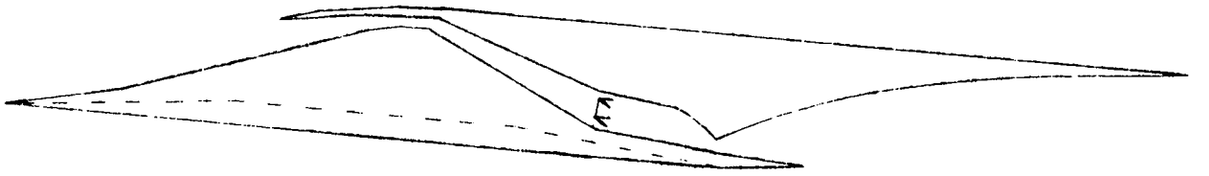

AU nozzle, ν = 66°

SY nozzle, ν = 65°

Figure 12.- Sketch of nacelles for optimum range utilizing 72° turning shortened nozzles.

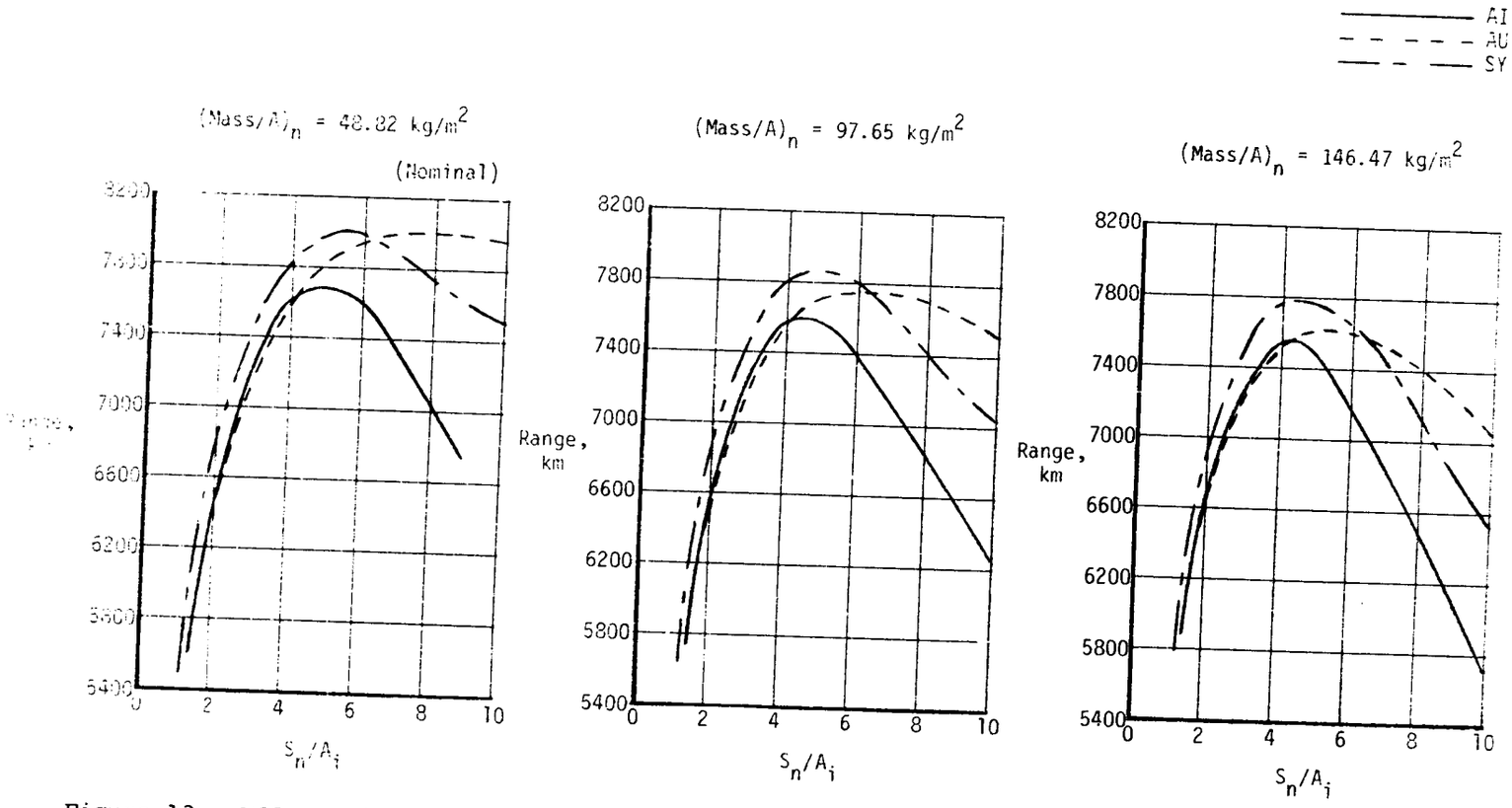

Figure 13.- Effect of nozzle mass per unit internal surface area on optimum range performance; $\nu = 72^o$, full-length and shortened nozzles.

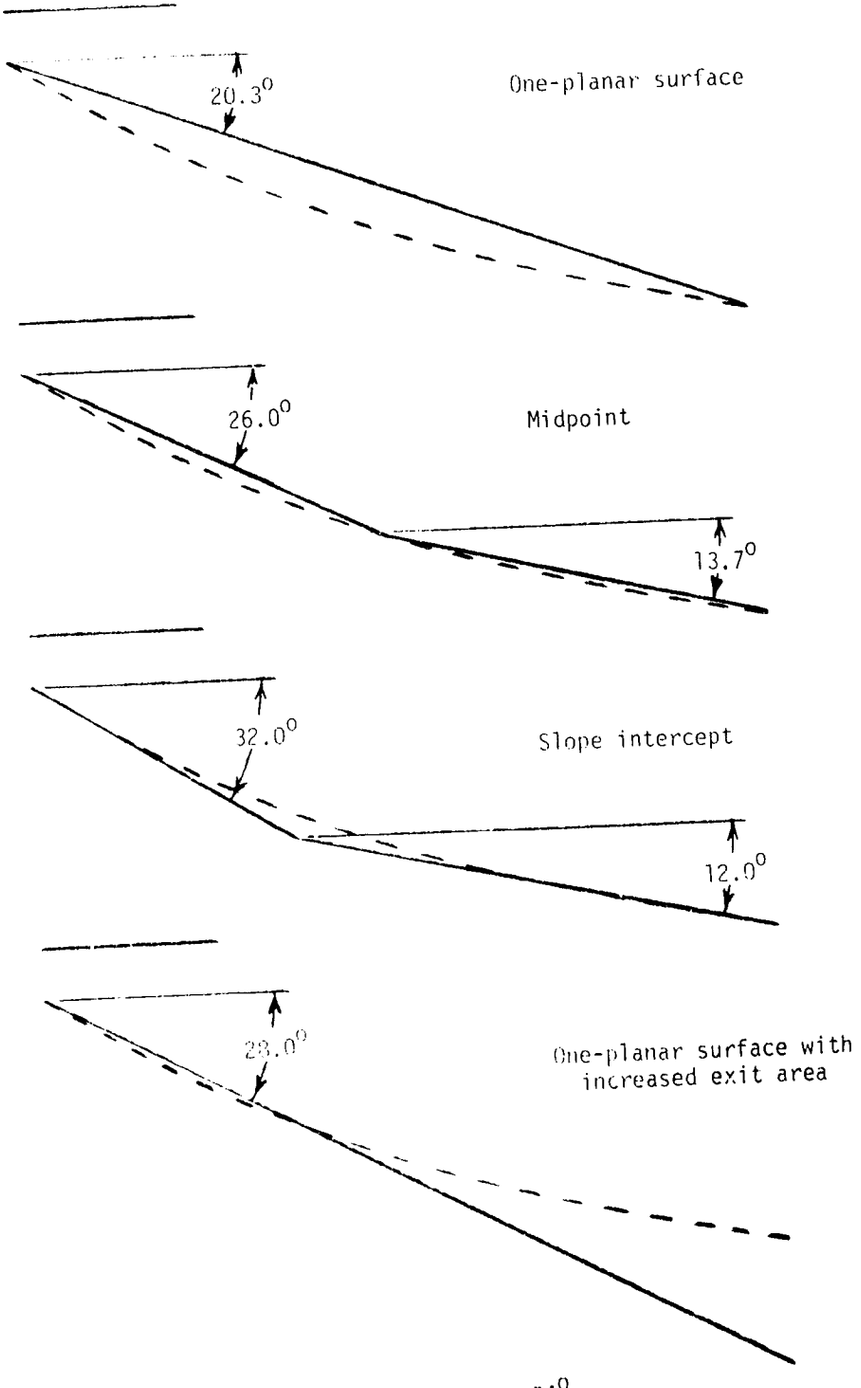

of 52 nozzle horizontal to = 54°

Figure 34.- Sketch of planar-surface nozzle approximations.

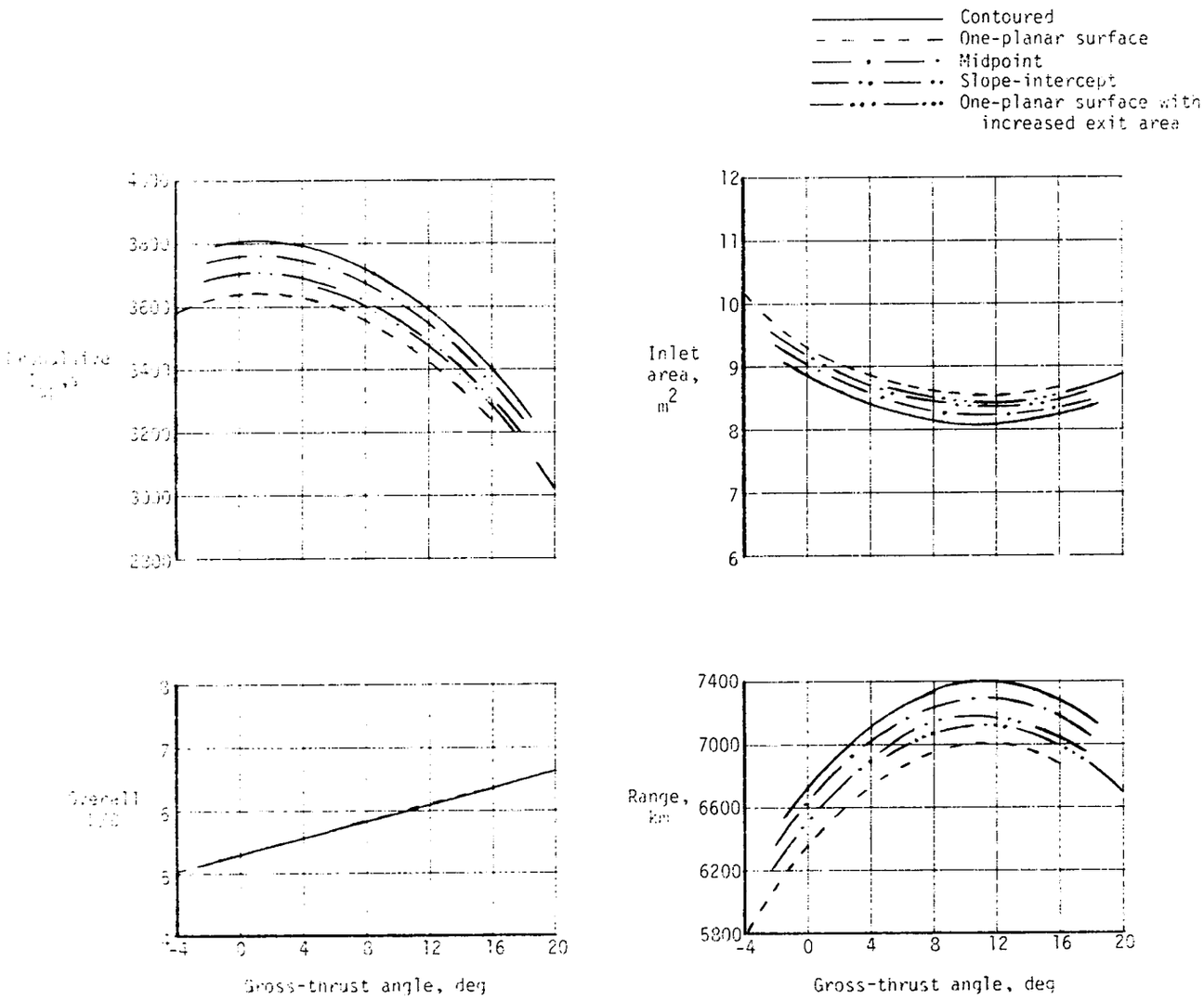

Figure 15.- Performance of planar-surface nozzle approximations; 64° AI nozzle shortened to $\nu = 54°$.

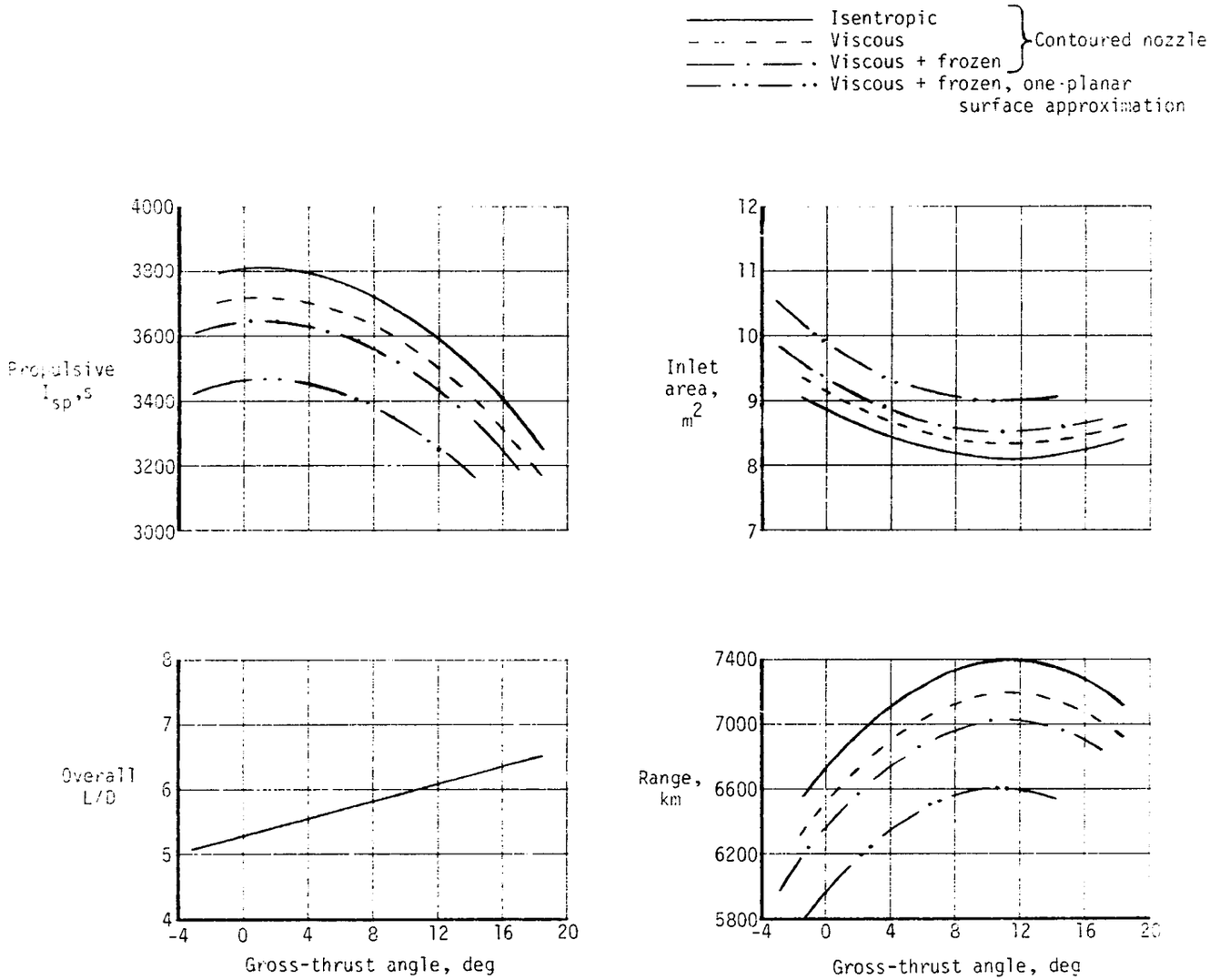

Figure 16.- Viscous- and frozen-flow effects on nozzle performance; 64° AI nozzle shortened to $\nu = 54°$.

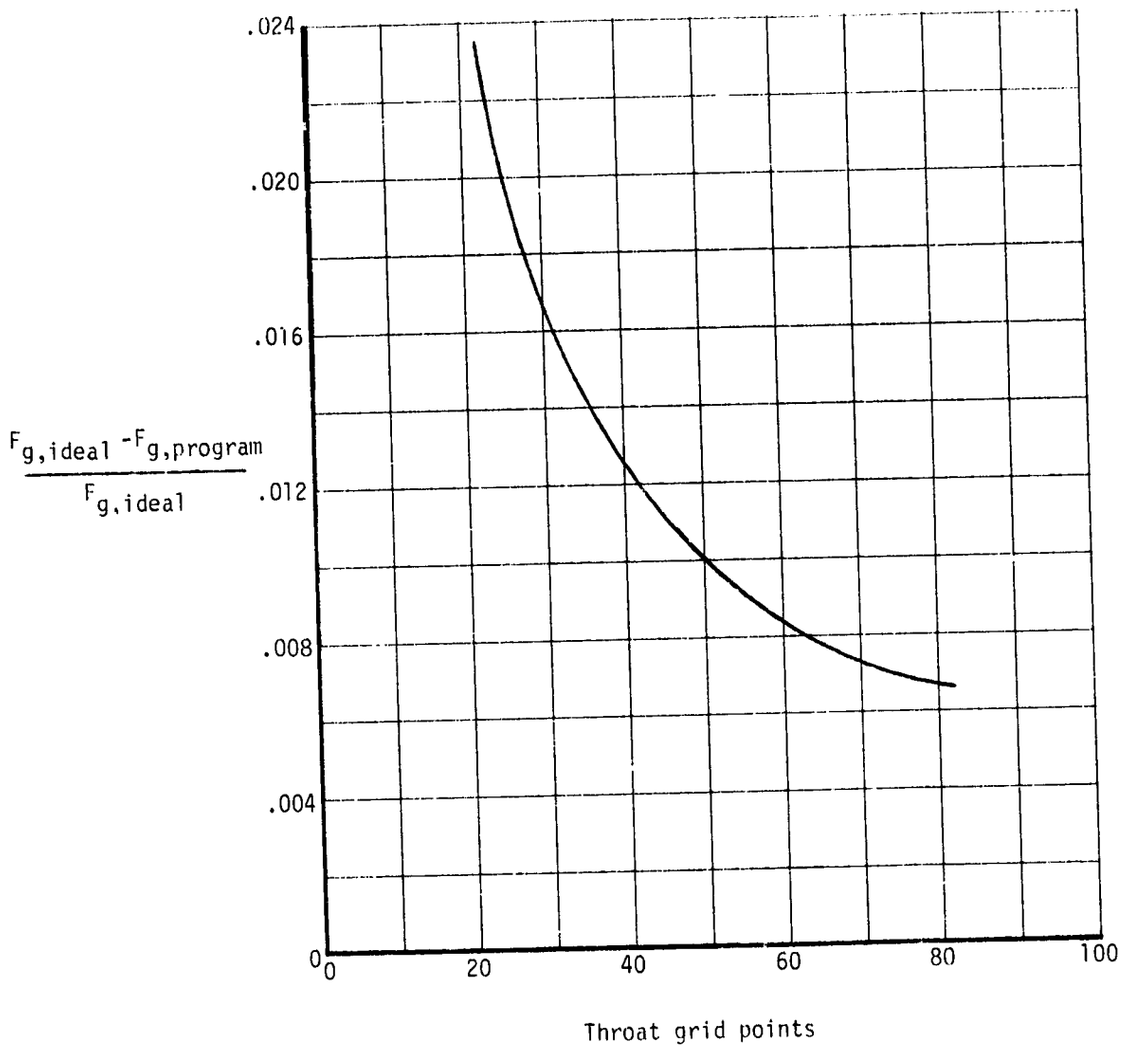

Figure 17.- Effect of nozzle computer-program grid spacing on gross thrust.

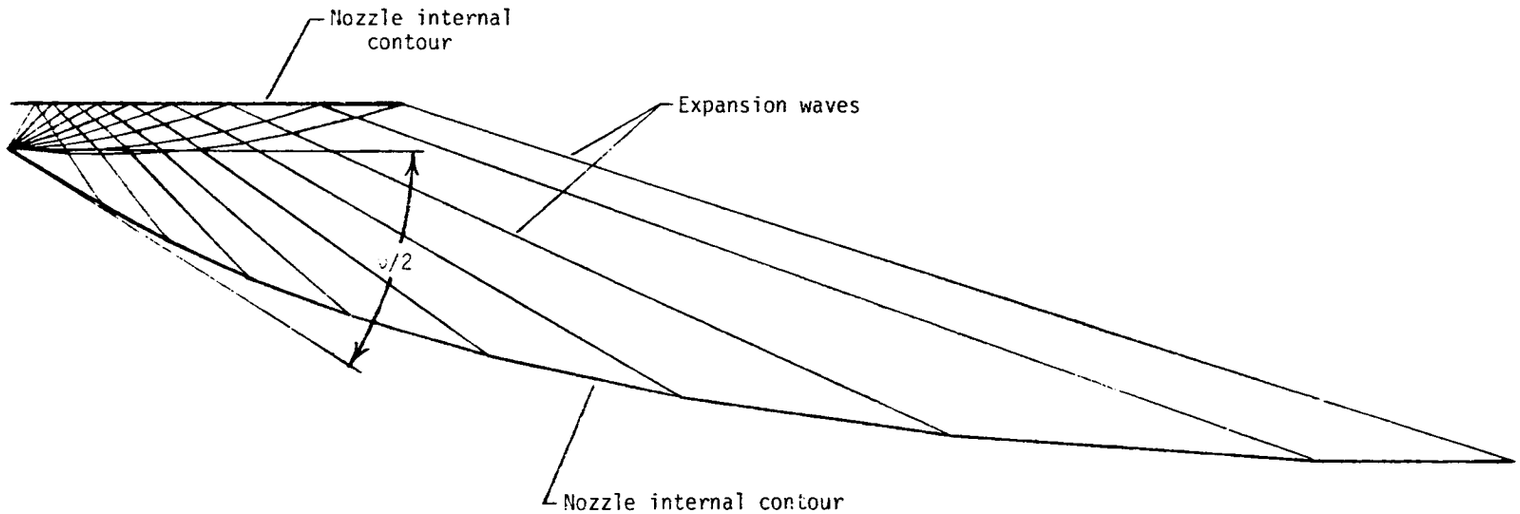

Figure 18.- Layout of 64°, total, internal-turning AI nozzle using Method of Characteristics.

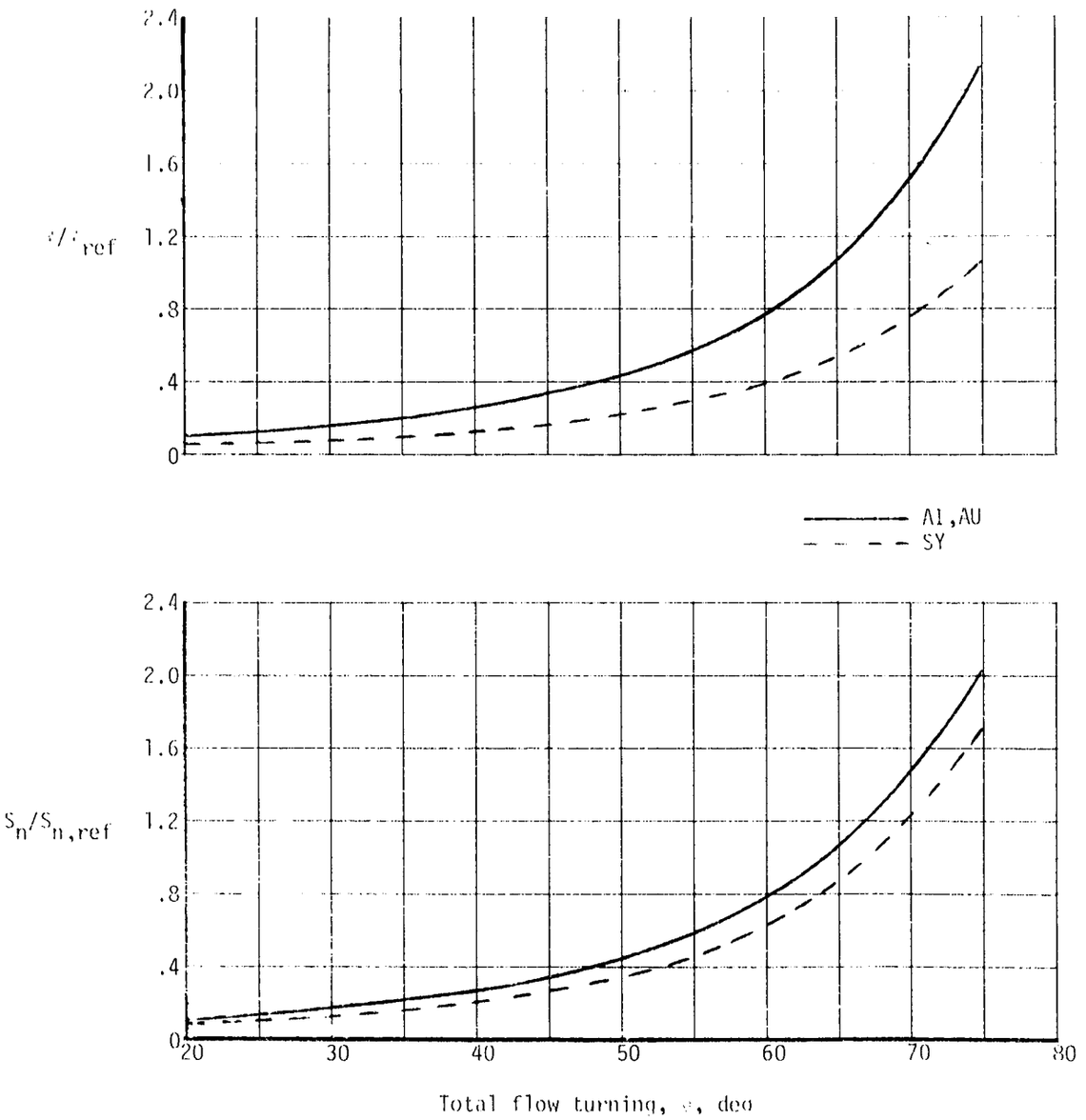

Figure 19.- Length and internal-surface area of uniform, parallel exit flow, isentropic nozzles.

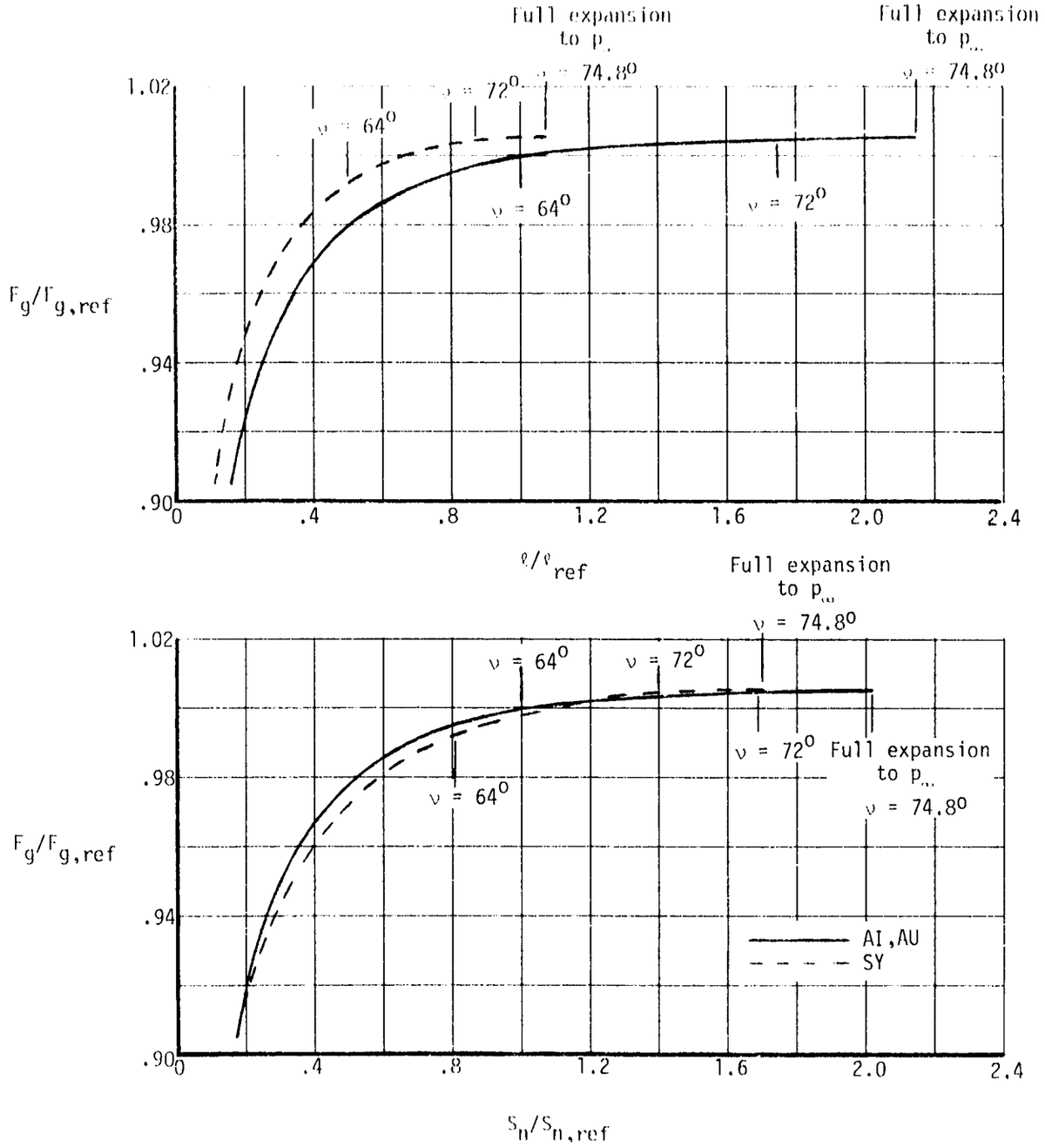

Figure 20.- Gross thrust of isentropic nozzles with uniform, parallel exit flow.

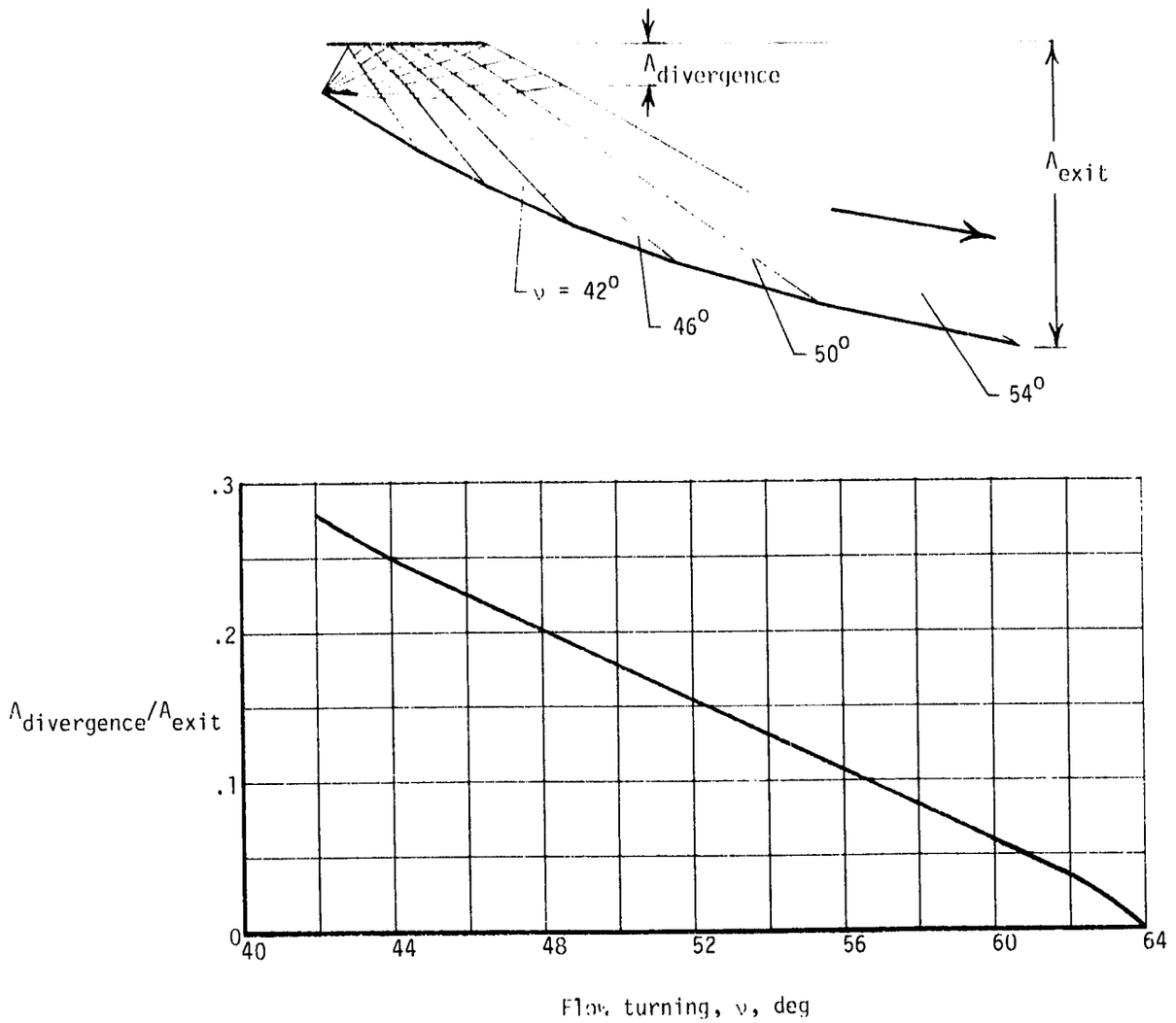

Figure 21.- Exit area affected by flow divergence for shortened, 64° turning AI nozzle.

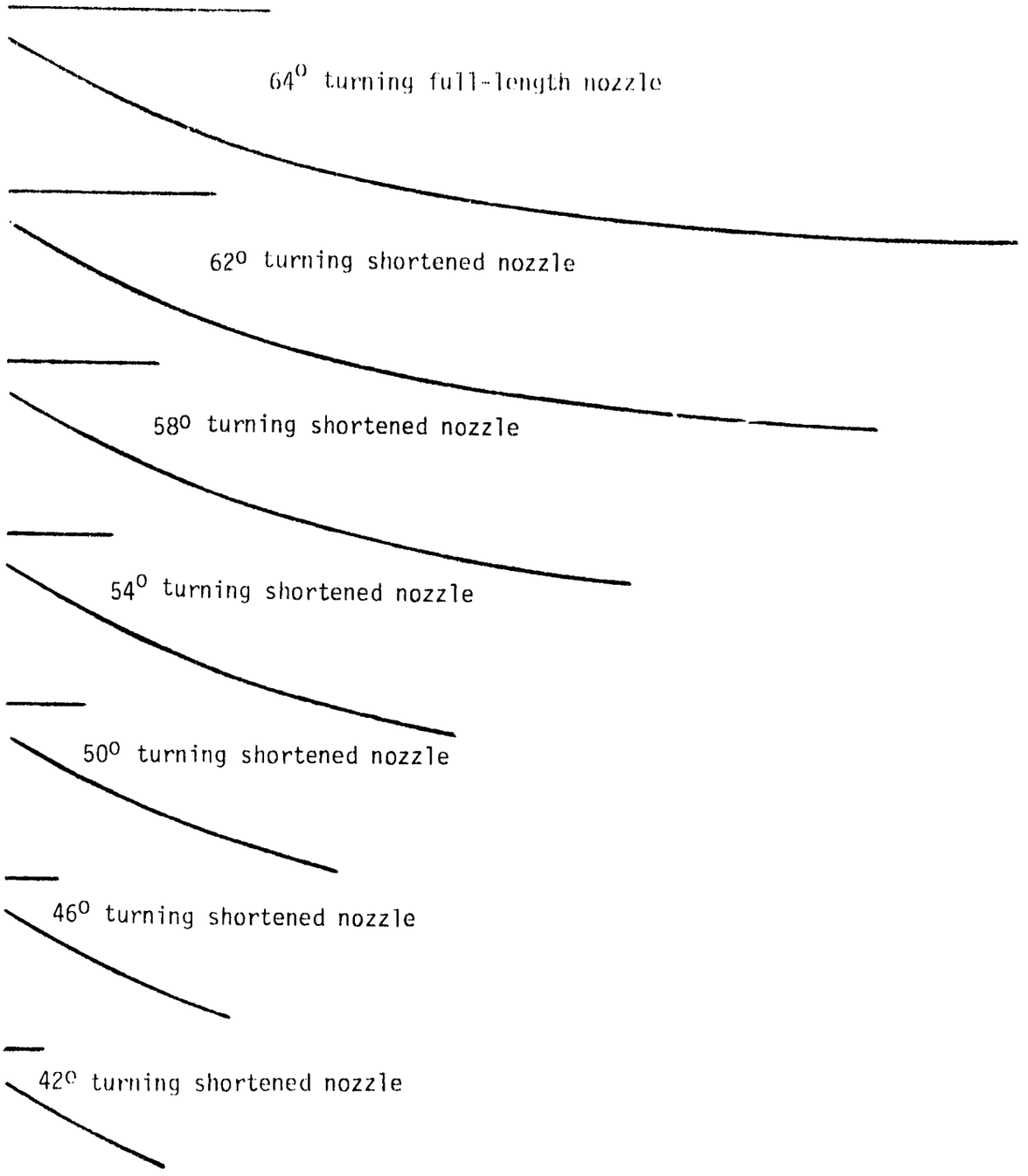

Figure 22.- Shortened versions of 64° turning full-length AI nozzle.

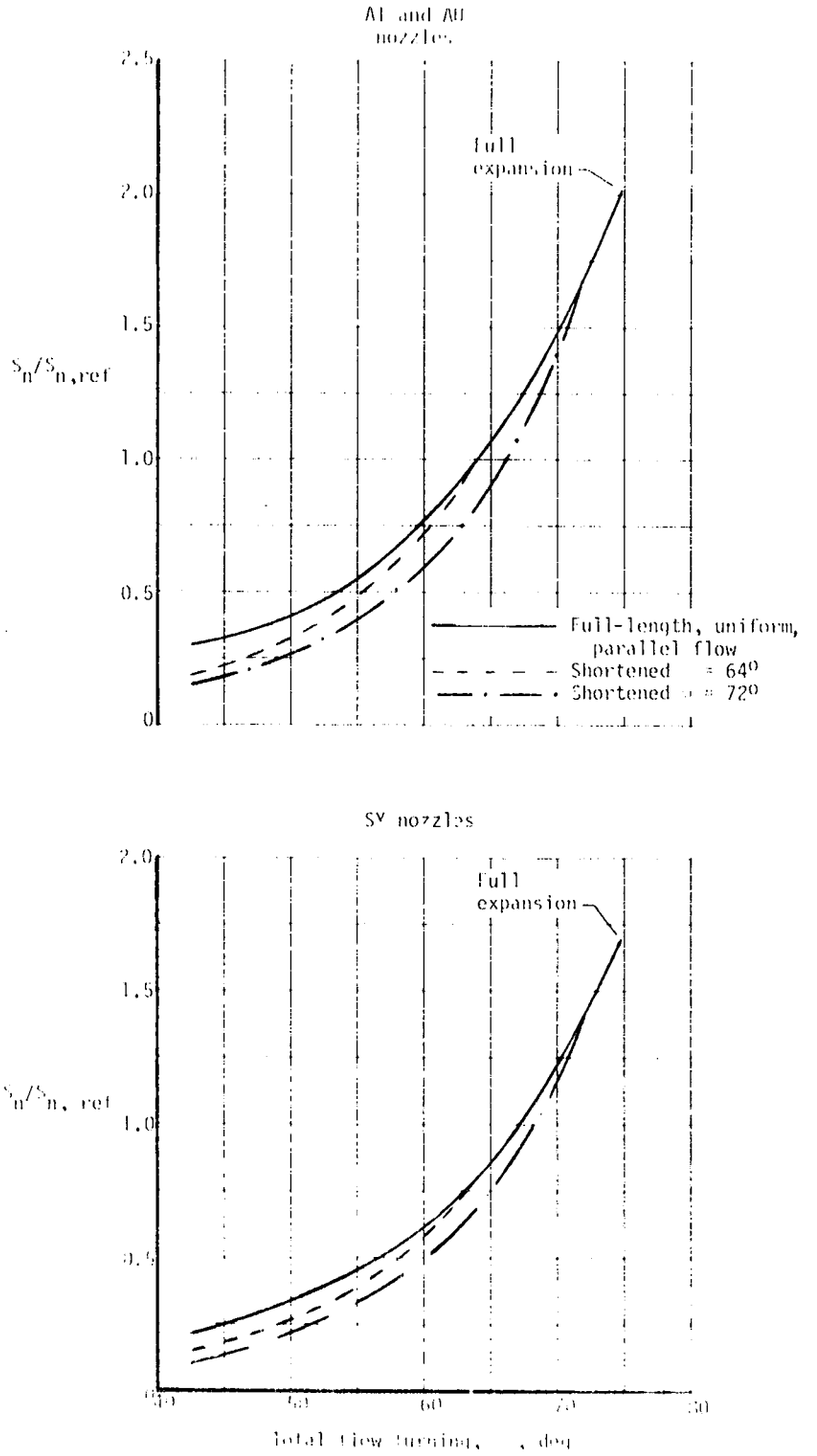

Figure 23.- Nozzle internal-surface area for full-length and shortened nozzles.

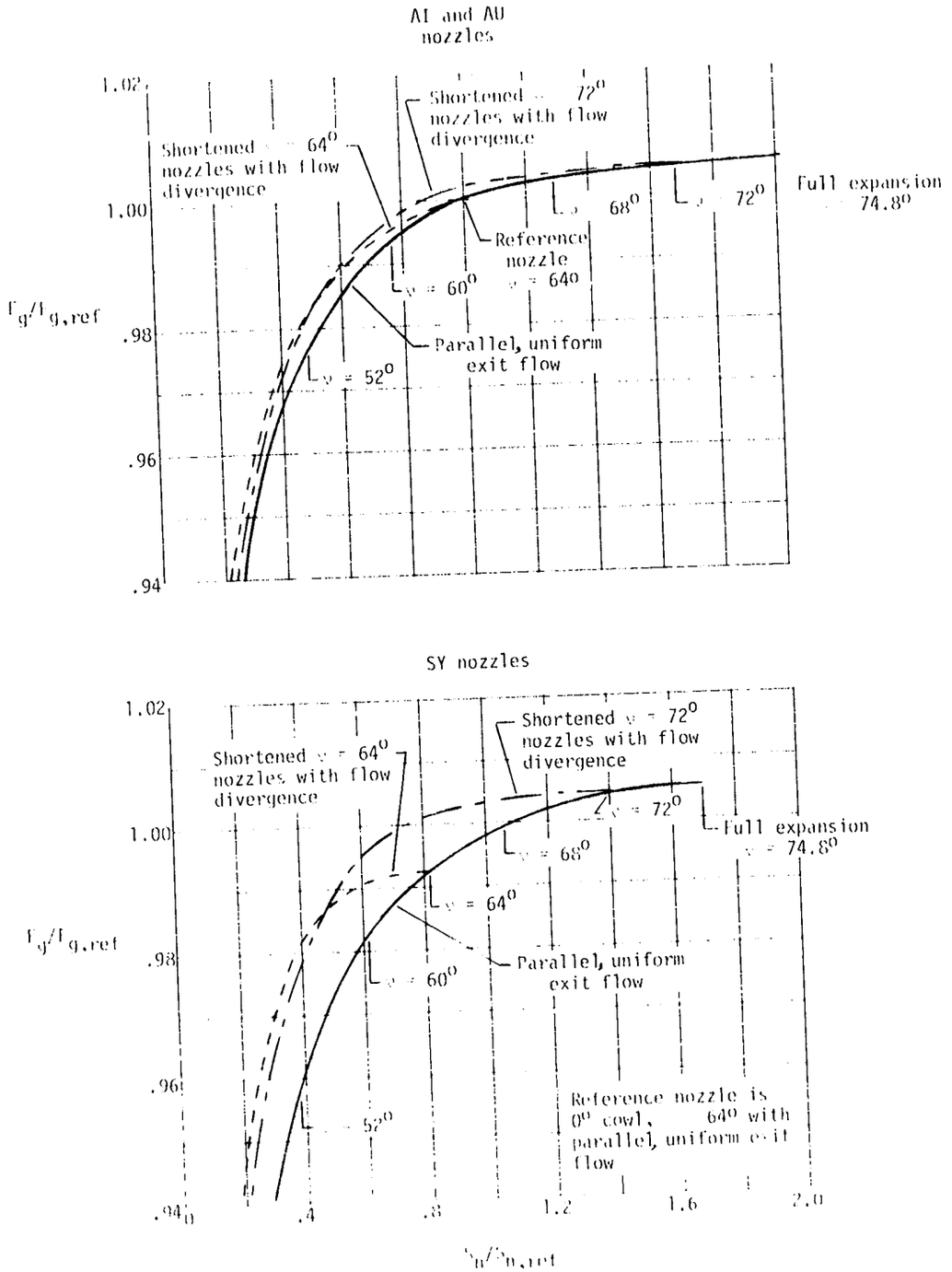

Figure 24.- Performance of AI, AU, and SY exhaust nozzles.